Photocatalytic Conversion of Carbon Dioxide to Fuel

Swati Aggarwal

Department of Biotechnology and Medical Engineering

National Institute of Technology Rourkela

Photocatalytic Conversion of Carbon Dioxide to Fuel

Dissertation submitted to the

National Institute of Technology Rourkela

in partial fulfillment of the requirements

of the degree of

Master of Technology

In

Biotechnology

by

Swati Aggarwal

(Roll Number: 214BM2380)

Based on research carried out

under the supervision of

Dr. P. Balasubramanian

May, 2016

Department of Biotechnology and Medical Engineering

National Institute of Technology Rourkela

Biotechnology and Medical Engineering

National Institute of Technology Rourkela

Dr. P. Balasubramanian

Assistant Professor

May 26, 2016

Supervisor's Certificate

This is to certify that the work presented in this dissertation entitled " Photocatalytic Conversion of Carbon Dioxide to Fuel" by "Swati Aggarwal", 214BM2380, is a record of original research carried out by him/her under my supervision and guidance in partial fulfillment of the requirements of the degree of Masters of Technology in Biotechnology from Department of Biotechnology and Medical Engineering at National Institute of Technology Rourkela. Neither this dissertation nor any part of it has been submitted for any degree or diploma to any institute or university in India or abroad.

Dr. P. Balasubramanian

Supervisor

Declaration of Originality

I, Swati Aggarwal, 214BM2380, hereby declare that this dissertation entitled ' Photocatalytic Conversion of Carbon Dioxide to Fuel' represents my original work carried out as a postgraduate student of NIT Rourkela and, to the best of my knowledge, it contains no material previously published or written by another person, nor any material presented for the award of any other degree or diploma of NIT Rourkela or any other institution. Any contribution made to this research by others, with whom I have worked at NIT Rourkela or elsewhere, is explicitly acknowledged in the dissertation. Works of other authors cited in this dissertation have been duly acknowledged under the section "Bibliography". I have also submitted my original research records to the scrutiny committee for evaluation of my dissertation.

I am fully aware that in case of any non-compliance detected in future, the Senate of NIT Rourkela may withdraw the degree awarded to me on the basis of the present dissertation

May 26, 2016 Swati Aggarwal

NIT Rourkela

Acknowledgment

I take this opportunity to express my gratitude and heartfelt thanks to every individual who has taken part in my work since from inception of idea to completion.

I am privileged to express my deep sense of gratitude and profound regards to my supervisor Dr. P. Balasubramanian, Assistant Professor, Department of Biotechnology and Medical Engineering for his esteem guidance and noble supervision during the hours of project from the needs of project to results of it. I would also like to acknowledge Dr. Priyabrat Dash, Assistant Professor, Department of Chemistry and Dr. Sirsendu Ray, Department of Biotechnology and Medical Engineering for their expert and sincere guidance.

I would also like to thank Departments of Ceramic Engineering, Life Science, Physics, Metallurgy and Chemistry who gave me access to their facilities and infrastructure.

I am extremely grateful to my seniors Ms. Leepika Rout, Ms. Basanti Ekka, Mr Balmiki, Mr. Aniket Kumar, Mr. Ezhil Venuswaran and Mr. K. Senthil Guru for their unceasing help and encouragement. I place on record, my sincere gratitude to my lab partners Mr. Nazimdhine Aly, Ms. Bunushree Behera, Ms. Jiku John and Mr. Bhaskar Das for their day-to-day support.

I would also like to express my gratitude to my colleagues Mr. C. R. Naveen Kumar Reddy and Ms. B. Abinaya for their constant help and encouragement in odd times.

Finally, I would like to express my love and respect to my parents for their encouragement and endless support that helped me at every step of life. Their sincere blessings and wishes have enabled me to complete my work successfully.

May 26, 2016 **Swati Aggarwal**

NIT Rourkela **Roll Number: 214BM2380**

Abstract

Carbon dioxide (CO_2) is a harmful greenhouse gas that is being increased in the atmosphere. As CO_2 emissions build up in the atmosphere, it tends to warm the climate leading to many adverse changes in atmosphere and thus causes various irreparable damages on our environment. This critical juncture compelled researchers to work upon converting this emitted CO_2 into fuel like methanol, butanol or even gasoline which can reduce the emission of GHG in the atmosphere. Photocatalytic approach to convert CO_2 into methanol in the presence of TiO_2, a photocatalyst has been very promising till date and discussed in this work. TiO_2. TiO_2 synthesis was done by two routes, hydrolysis and sol-gel. In hydrolysis method, various concentration from 1 mol.dm-3 to 3 mol.dm-3 and volume from 50 ml to 200 ml. Anatase phase increased with the increase in volume. The same was the trend in increase of photoluminescence. Sol-gel proved to be a better photocatalyst with a lower size range of 40-60 nm than hydrolysis method that range from 40-90 nm. The photo reduction of CO_2 with H_2O was efficaciously demonstrated in a laboratory scale photoreactor with TiO_2 and TiO_2-Nb catalysts. The maximum methanol yield amongst all the catalysts was 0.15 μgm/ml by using TiO_2 (sol-gel) under UV irradiation. Compared with other catalysts proved to be a better photocatalyst. Doping had no positive impact on photoreduction of CO_2 to methanol. All in all, a successful demonstration of material synthesis and its application in photoreduction of CO_2 was achieved.

Keywords: CO2 emission; Photocatalytic approach; Hydrolysis and sol-gel method; Niobium Doping, Photoreduction, Methanol Production

Table of Contents

List of Figures

List of Tables

Chapter 1

Introduction

1.1. Background

Carbon dioxide (CO_2) is a greenhouse gas (GHG) emitted through various anthropogenic actions, primarily combustion of fossil fuels for various purposes like transportation and industrial processes. With the urbanization CO_2 amount in atmosphere has increased. As per UN Statistics division, 32,000 tons of CO_2 is added every 60 seconds to the atmosphere. CO_2 takes part in changing the climate change by raising the global temperature due to absorbing infra-red light and re-emitting it. The enhancement of CO_2 is primarily due to excessive burning and use of fossil fuels and deforestation. CO_2 sources can be divided into concentrated and diluted streams. Concentrated sources are CO_2 reservoirs and exhaust gases from various industrial plants. Diluted sources can be plants used for processing of natural gas and various chemicals manufacture like ammonia. The energy sector is accountable for almost 25% of the global CO_2 production. Additionally, 10-30 % of CO_2 emission is due to deforestation and combustion of fossil fuels [1].

While various natural sources cause CO_2 emissions, human related emissions are majorly responsible for the increase that has occurred in the atmosphere. As GHG emissions build up in the atmosphere, climate tends to warm leading to many adverse changes in atmosphere and thus causes various irreparable damages on our environment. This highly impacts the plant ecology and the well-being of humans [2]. Increase in CO_2 emissions affected the quantity and seasonality of pollens. Augmented CO_2 stimulates production of pollen more than its overall growth and the produced pollen is highly allergenic. This elevated plant based respiratory diseases like asthma, cardiac distress, anaphylaxis, inflammation of nasal membranes, sneezing and wheezing. Food security is another key aspect of world health. When exposed to higher temperature plants may have adverse effects on fertilization or fruit formation during their reproductive stage. Moreover, water supply for irrigation would become a serious issue with declining snow and ice reserves on mountains. Ultimately, human health is imposed to risk due to affected plant biology by climate change and increased CO_2 emissions.

With the recent changes in climate, measures are being taken to limit the CO_2 emission such as capture and underground storage; use as solvent in supercritical form; improve preservation of beverage in food industry and maintain cell and microorganism viability in small scale of application. In spite of the numerous efforts, still CO_2 emissions take place at the rate of one part per million (ppm) every year, and as per International Panel on Climate Change (IPCC), now it has turned out to be 407.12 ppm that ever existed during 8,00,000 years. This critical juncture compelled researchers to work upon this global issue and develop a cost-effective, revolutionary technology. They came up with converting this emitted CO_2 into fuels like methanol, butanol or even gasoline and various chemical products which can reduce the emission of GHG in atmosphere.

Researchers from multidisciplinary fields whether it is nanotechnology or chemical or mechanical or if it is biotechnology, all are working on artificial photosynthesis to reduce our dependence on crude oil and utilize manmade CO_2 emissions. In past few years, various technologies like photocatalytic, thermochemical, electrochemical, biochemical and microbial technologies came into existence. Figure 1.1 describes the most current and potential uses of CO_2. CO_2 usage is divided into two groups, pertaining to its physical and chemical properties [3]. Physical applications include beverage industry, supercritical CO_2 extraction and enhanced oil recovery. CO_2 being a safe gas is used in fire extinguishers and food preservation. In the chemical applications, CO_2 is a reactant and used in the processing of chemicals like salicylic acid and methanol. It is used to manufacture calcium carbonate ($CaCO_3$) and sodium bicarbonate ($NaHCO_3$) in organic industry. It is also used in biomass production for plants during photosynthesis. In all, only 0.7 – 1.0 % of the CO_2 is being used at present.

CO_2 conversion including chemical transformation, electrochemical reduction, photocatalytic reduction, biological and biochemical conversion, etc., has been well documented in several literatures [4]. Among these, conversion of CO_2 to fuels or useful chemicals with the help of sunlight is a good alternative but a thought-provoking process. CO_2 photo reduction involves multi-electron processes that lead to a large range of products from CO, CH_4 to alcohols, aldehydes 6]6+9*--and carboxylic acids. But most difficult step is the breaking of water molecule to yield hydrogen. The most ideal route would be the reduction of CO_2 and H_2O by Fishcher-Troph's process to give higher hydrocarbons. This can be achieved by activation of photocatalysts in

presence of various sources of light energy. When compared to other systems, photocatalytic system is simpler and easy to build, thus, highly preferred technology over others. It is abundant, clean, safe, cheap and gaining researchers attention due to harnessing of solar energy.

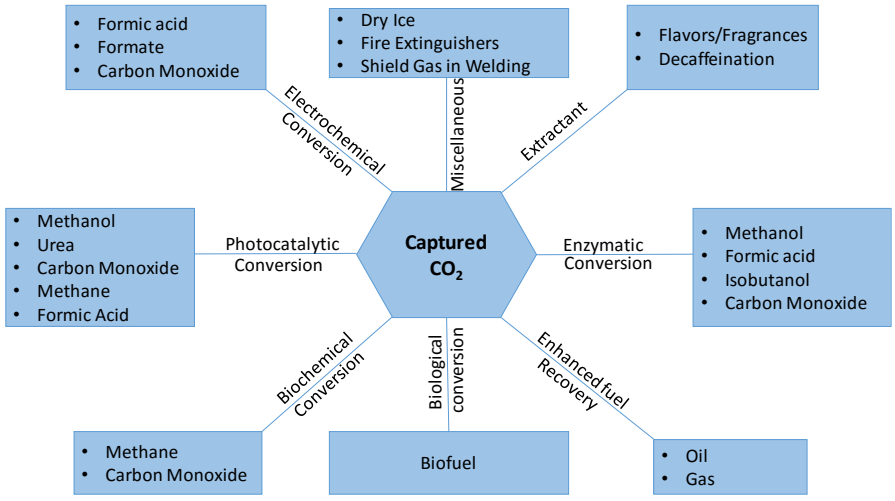

Figure 1.1: The most current and potential uses of CO_2

1.1. Aim and scope of current study

Photocatalytic reduction of carbon dioxide to fuels and numerous other products is an evolving research area in order to reduce CO_2 and utilize abundant sunlight in the atmosphere. It can prove to be a potential supplement of energy in future. Though, many challenges are being faced by researchers, some of them are as follows:

- The overall process centers around the two most important and stable molecules of chemistry, water and CO_2.
- Breaking water and CO_2 molecules is one of the toughest step in this process.
- Conversions achieved to date is very small (<1%).
- Design of photocatalyst, selection of a metal or non-metal ion for doping also makes the process complex.
- Sometimes, photocatalyst deactivates for a short duration.

Thus, design of efficient photocatalysts and achieving higher yield of desired products are the two key issues that researchers are being focused upon round the globe.

The primary objective of the current research is to explore new catalyst systems to improve the photocatalytic reduction of carbon dioxide to fuel. Catalyst should have two general

characteristics, one is the photocatalytic hydrogen splitting and other is the reduction of CO_2 to hydrocarbons. To achieve these goals, a catalyst should also have a negative reduction potential with respect to CO_2.

One of the most studied semiconductor is TiO_2, still researchers are working on improving the yield of photo reduction of CO_2 with water. Doping of TiO_2 with niobium would be employed in this project to enhance the photocatalytic efficiency. It has been observed that TiO_2-Niobium composite has not been reported for photocatalytic reduction of CO_2. Hence, it has been selected for studies in this work.

The following are the objectives of the study:

- Studies on TiO_2 samples prepared by two different synthesis routes, hydrolysis and sol-gel route.
- Preparation of TiO_2-Niobium composite and study the effect of niobium (Nb) metal loading on titania by studying the photocatalytic properties.
- Comparison of TiO_2 and composite of TiO_2-Niobium semiconductors activities for their abilities to photo catalytically reduce CO_2.
- Characterization and estimation of methanol produced by photo reduction of CO_2.

A better catalyst system by means of above research is expected from this study. This would enhance the understanding and their implication in the photocatalytic reduction of CO_2 to higher alcohols or any other useful products.

Chapter 2

Literature Review

2.1. CO_2 – A Harmful Greenhouse Gas

Carbon and oxygen are the elements that are found all over the world. When combined with a double bond, they produce CO_2, an odorless and colorless gas (O=C=O). It was recognized as a gas in the 17^{th} century by Jan Baptista van Helmont, a Belgian chemist. It liquefies upon compression and partially freezes to dry ice, if allowed to expand upto atmospheric pressure. CO_2 converts to carbon monoxide and oxygen at high temperatures. It can be solubilized in water to give a weak acid solution called as carbonic acid (H_2CO_3). It can be used as a fire extinguisher, refrigerant, foaming rubber, carbonated beverages and in slaughter house to immobilize animals. It has a crucial importance in photosynthesis of plants. The structure of CO_2 is described in Fig. 2.1. Apart from advantages, CO_2 is a heat-trapping greenhouse gas that inhibits radiant energy from the earth to go back to space, thus heating the environment and causing changes in the climate.

Major sources for CO_2 increase in the atmosphere are burning of fossil fuels. Increasing CO_2 leads to global warming, thus CO_2 mitigation has become an utmost need. Several strategies to achieve this are being employed, among them, CO_2 capture and sequestration technologies are generally being taken as viable and efficient ones. Though, these technologies are costly and require high energy input, thus making them economically non-profitable. These technologies are good at large scale but at the same time, other technologies must be used to convert captured CO_2 into useful products. Various other technologies like gas adsorption into chemical solvents, cryogenic distillation and permeation through membranes are employed for the sequestration of CO_2 from the industrial gas [4]. But the most oxidized form of carbon is CO_2, thus, reduction is the only chemical transformation at normal energy. For this purpose, a broad spectrum of CO_2 transformation techniques is under investigation including chemical, photochemical, thermochemical, radiochemical, electrochemical, biochemical, bio-photochemical and electro-photochemical conversion [5].

2.2. Thermodynamics behind CO_2 conversion to fuel

CO2 is a very stable molecule and breaking its bond is a time and energy consuming process. Highly optimized reaction conditions, active catalysts and large amount of energy is required to break the strong carbon oxygen bonds. [6]. However, the most important factor driving any chemical reaction is the Gibbs free energy required to convert reactant into product. This can be represented by Gibbs-Helmholtz relationship:

$$\Delta G^\circ = \Delta H^\circ - T\Delta S^\circ$$

Both the factors (ΔH° and TΔS°) are not favorable in reducing carbon dioxide to fuel or any other product. Due to linearity of CO_2 molecule with two reactive sites (oxygen and carbon), it is highly stable with Gibb's free energy of ΔG°= -394.38 kJ mol^{-1}. Due to this high energy input, entropy (TΔS°) makes no contribution to the thermodynamic driving force but enthalpy (ΔH°) can act as an initial guide to assess thermodynamic constancy of CO_2 conversion reaction. A graph representing CO2 activation is given in Figure 2.1. ΔG° is highly positive in all the reactions involved in conversion of carbon dioxide to fuel. For example, steam reforming of methane to give carbon monoxide and hydrogen:

$$CH_4 + CO_2 \rightarrow CO + 3\,H_2 \qquad \Delta H^\circ = +206.3 \text{ kJ mol}^{-1}$$

The heats of reaction play an important role for CO production when CO_2 is a single reactant. When CO_2 is a co- reactant with other reactant of higher Gibb's free energy (eg. H_2 and CH_4), these reactants donate their chemical energy to stimulate CO_2 reduction. For example:

$$CO_2 + 3CH_4 + O_2 \rightarrow 4CO + 6H_2 \qquad \Delta H^\circ = +165.8 \text{ kJ mol}^{-1}$$

Moreover, metal complexes, nitrogen-containing compounds, polycarbonates and nanomaterials could favorably react with CO_2. Hydrogenation of CO2 to methanol, formic acid and methane would be possible through C-H bond formation. Perhaps, this mechanism can be used for production of fuel by using CO_2 chemically. Almost, 95 percent methane conversion occurs by this process [7].

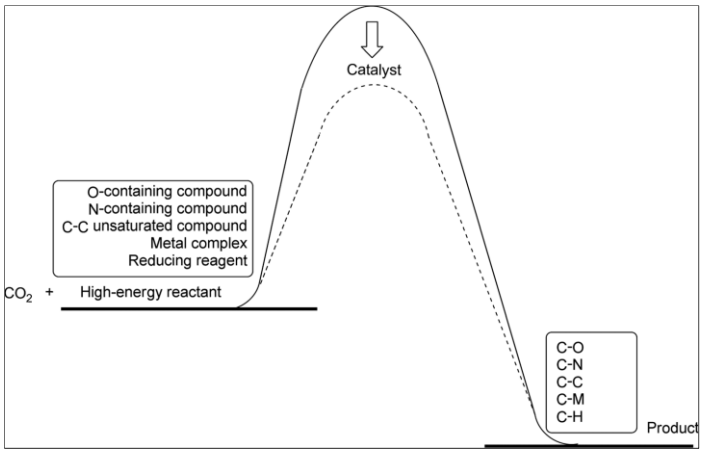

Figure 2.1: A graph representing CO2 activation

2.3. CO_2 management and sequestration technologies

With time, numerous technologies came to reduce CO_2 in the atmosphere. Most conventional was the sequestration of CO_2 in rock beds and underneath the earth. Few other were adsorption in solvents and penetration through membranes. But these techniques didn't prove to be fruitful, so the conversion of CO_2 by various pathways came into existence. The chemical reactions involved in various reduction pathways are described in following equations [8].

- Chemical Reduction by metals

$$\mathbf{2\,Mg + CO_2 \rightarrow 2\,MgO + C} \qquad 2.1$$

- Thermochemical conversion

$$\mathbf{CO_2 \xrightarrow{Ce^{4+}} CO + \frac{1}{2}\,O_2} \qquad 2.2$$

- Photochemical conversion

$$\mathbf{CO_2 \xrightarrow{h\nu} CO, HCHO} \qquad 2.3$$

- Radiochemical conversion

$$\mathbf{CO_2 \xrightarrow{\gamma\ radiation} HCOOH} \qquad 2.4$$

- Electrochemical conversion

$$\mathbf{CO_2 + xe^- + xH^+ \xrightarrow{eV} CO, HCHO} \qquad 2.5$$

- Biochemical conversion

$$\mathbf{CO_2 + 4H_2 \xrightarrow{bacteria} CH_4 + 2H_2O} \qquad 2.6$$

- Biophotoelectrochemical conversion

$$\mathbf{CO_2} \xrightarrow{\mathbf{h\nu,enzyme}} \mathbf{HCOOH} \qquad 2.7$$

Among all the above approaches, photo catalysis seems to have an added advantage and more attractive method for the reduction of CO_2 in the atmosphere.

2.4. Photo catalysis approach and its principle

The photo catalysis approach for reduction of CO_2 is of great interest in terms of theoretical and applied photochemistry. It is a thermodynamic process where standard free energy ($\Delta G°$) of formation is -394.359 kJ/mol. In 2050 carbon dioxide emission scenarios, it has been predicted that direct solar energy (3×10^{19} $Jy^{-}1$) would be the top renewable technology [9]. Thus, an economical production of CO_2 is likely only if sunlight is used as a source of energy. After selection of source of energy, the next important task is the combination of two processes of water splitting and carbon dioxide reduction. This could be done in presence of a semiconductor. Numerous semiconductors are being discovered for this purpose that will be discussed in the later part of the thesis. Before that basic principle of photo catalysis would be discussed here.

When light is illuminated on any semiconductor or a photocatalyst, an energy interval is created between its conduction and valence band, known as band gap. The valence band (VB) is the highest energy band occupied with electrons and conduction band (CB) is the lowest energy band without electrons. Once the light with energy content higher than the band gap is irradiated on semiconductor, electrons are transferred to CB from VB. The movement of electrons lead to redox potential due to generation of electron-hole pairs. This scenario is called as the 'photoexcitation state' of the semiconductor. The negative e^- reacts with the O_2 molecule to give an oxide anion and the positive hole reacts with the water molecule to give hydroxyl radical. A schematic representation of the photocatalytic process is given in Figure 2.2.

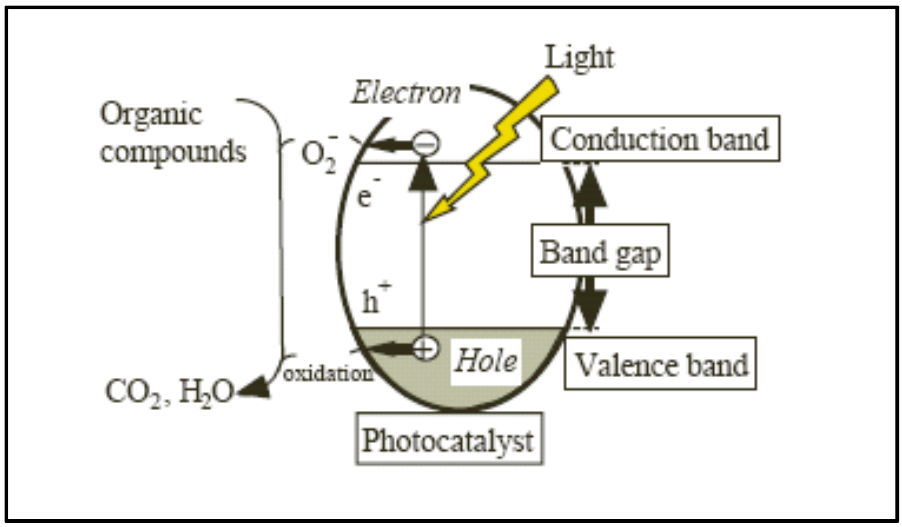

Figure 2.2: Mechanism of photocatalytic process

The rate of a photocatalytic reaction depends upon following factors [10]:

- Concentration of the substrate
- Temperature that cause collision between the substrate and the photocatalyst
- pH of the medium
- Reaction on the substrate of the semiconductor
- Diffusion of the products from the surface of the semiconductor

CO_2 photo reduction is a multi-step process wherein CO_2 reduction and water splitting takes place simultaneously. Initial step in the CO_2 reduction is the formation of e^--h^+ pairs. The rate of e^--h^+ recombination is two to three times faster than other electron transfer processes. Henceforth, processes inhibiting e^--h^+ recombination would highly enhance the proficiency and rates of CO_2 photo reduction.

Reactions for one, two, four, six and eight electron reduction potentials for CO_2 reduction and H_2O oxidation at pH 7 and room temperature are as follows [11]:

Reaction	E_{redox}
$\mathbf{2H^+ + 2e^- \rightarrow H_2}$	-0.41
$\mathbf{H_2O \rightarrow \frac{1}{2}\, O_2 + 2H^+ + 2}e^-$	0.82
$\mathbf{CO_2 + e^- \rightarrow CO_2^-}$	-1.9
$\mathbf{CO_2 + 2H^+ + 2e^- \rightarrow HCO_2^-}$	-0.50
$\mathbf{CO_2 + 2H^+ + 2e^- \rightarrow CO + H_2O}$	-0.54

$\mathbf{CO_2 + 4H^+ + 4e^- \rightarrow HCHO + H_2O}$ -0.49

$\mathbf{CO_2 + 6H^+ + 6e^- \rightarrow CH_3OH + H_2O}$ -0.39

$\mathbf{CO_2 + 8H^+ + 8e^- \rightarrow CH_4 + 2H_2O}$ -0.25

From the above reactions, it is evident that CO_2 photo reduction is a multi-photon process. Thus, any process inhibiting this e^--h^+ recombination would greatly enhance the efficiency of CO_2 photo reduction. With the movement of one electron, the structure converts to bent from linear resulting in irreversible reduction. This electron transfer is endergonic because of high negative adiabatic electron affinity of CO_2. The kinetics of above reaction depends on numerous aspects such as intensity of incident light, amount of light absorbed by catalyst, surface area and charge of photo catalyst, reaction temperature, reactant adsorption, product desorption and CO_2 activation [10].

2.5. Nanomaterials and their role in photo catalysis

The terminology 'Nanotechnology" was first coined by Norio Taniguchi, Tokyo Science University in 1974. It deals with the study of structures in size range of 1 to 100 nm. It involves development of devices and materials in the nano range. Nanotechnology enable us to prevent and detect contaminants in air, soil and water in a very cost-effective manner. It has implications in all sectors whether it is agriculture and food, energy and environment, cosmetics or the medical instruments and drugs [12]. It is truly a multi-disciplinary and an emerging technology with an influence on the civilization and breakthroughs in near future.

One of the best application of nanomaterials is in photocatalytic conversion of carbon dioxide to fuel. Numerous synthetic semiconductor systems have been in proposed in literature for this purpose. The most deeply researched systems are semiconducting materials, especially TiO_2. Inoue et al were the first who reported the photo catalytic reduction of CO_2 in aqueous solutions to give a combination of formic acid, formaldehyde, methane and methanol using wide-band-gap semiconductors such as titanium dioxide (TiO_2), tungsten trioxide (WO_3) and zinc oxide (ZnO) [13]. These semiconductors were suspended in water and activated by illumination of both xenon and mercury lamp. The concept of transfer of charge at photo excited semiconductor was followed to elucidate the photocatalytic reaction kinetics.

2.5.1. TiO_2 as a photo catalyst

TiO_2 is a commonly used semiconductor system for photo reduction of CO_2 due to its high stability, economical price, wide band gap, high availability and low toxicity [11]. It seems to be a

distinguishing candidate. Advances have been made to these systems with the dawn of semiconductor nanoparticles which cause an increase in the surface area of a semiconductor catalyst. This lead to an increase in the frequency between CO_2 and TiO_2, a crucial factor for the electron transfer reduction reactions. TiO_2 morphology and crystal structure studies are well explored in the literature in order to increase its photocatalytic activity.

By changing the morphology of TiO_2, electron transport through the nanomaterial could be controlled. The most studied morphology is the porous arrays or spheres which gave high yield of products. For instance, the conversion rate for CH_4 is 0.48 mmol/ (gcat h) over Pt (0.15wt%)/ TiO_2 nanotube arrays and 0.10 mmol/ (gcat h) over Pt (0.12wt%)/ TiO_2 nanoparticles [14]. Li et al synthesized MgO-TiO_2 patches which suffered problems of electron recombination which was later improved by changing patches to nano rod /wire configuration [15]. This resulted in minimization of electron hole recombination. Preparation methods play an important role in product selectivity and CO_2 reduction. It has been observed that TiO_2 prepared by sol-gel routes had higher selectivity towards ethanol than prepared by hydrothermal routes that yields formic acid. Sol-gel route synthesized titania yield methane and methanol as major product [16]. The catalyst dose used in reaction also have significant role in efficient CO_2 conversion. Reaction rate increases with the increase in catalyst dosage in the process. Though, disproportionate loading may induce unfavorable light scattering and low penetration of light might occur. The study of photocatalytic reduction of CO_2 with TiO_2 concentration between 0.1% and 2% w/v under 350nm light shows that 0.1% w/v TiO_2 suspension is optimum to reach ideal value of methane production [17]. Crystallite size tends to impact photocatalytic behavior of TiO_2. The anatase phase is said to be more reactive phase than the rutile phase. This might be due to enhanced hole capture that raised from bending of band gap.

Though the switch from semiconductor powders to semiconductor nanoparticles has effectively increased the surface area of TiO_2 catalytic systems, few additional modifications to TiO_2 are required to improve activity which restricts excitation to the UV range. Furthermore, modifications to reduce e^-–h^+ recombination rates and increase CO_2 availability at the catalyst surface must be done.

2.5.2 Modification of TiO_2 semiconductor system

In oreder to activate, TiO_2 require high energy input which is present in UV region of solar spectrum. Thus, it is desirable to synthesise photo catalysts that utilize visible region in a wider

region. The various methods to introduce visible light activity of TiO_2 are doping, dye-sensitization or composite semiconductors. In terms of metal doping, transfer of electrons takes place from CB to metal. Though, in case of dye-sensitized method, excited electrons are transferred to large band gap from small band gap dye and then injected into the CB of TiO_2.

Most common alterations made to TiO_2 include doping of the TiO_2 lattice with metal and nonmetals, leading to reduced e^-–h^+ recombination rates and visible sensitivity, respectively. Various doping techniques are metal ions that include impregnation, co-precipitation, sol–gel methods, metal–ion implantation and RF magnetron sputtering techniques. Doping of TiO_2 catalysts with metals (Rh, Pd, Pt, Cu, Ag, Fe, Cr, etc.) for CO_2 reduction are broadly accepted for further investigations by scientists.

This can be explained by considering the metal dopants as sinks for the excited TiO_2 electrons. When the excited electron is introduced into the CB of the TiO_2, it starts to travel through the TiO_2 crystal lattice and trapped by the metal dopants because of the relative lower energy state. Thus the metal dopant serves as a mean to separate the excited electrons from the holes that are in the TiO_2 lattice, thereby reducing e^-–h^+ recombination.

Using optimum amount of Cu-loading i.e. 2.0 wt %, methanol yield was increased to 118 µg/mol with 6h of illumination [18]. Compared to Ag–TiO_2, Cu–TiO_2 has higher photo activity as Cu metal act as electron trapping site and maintains the movement of photoelectrons at the same time. On the contrary, excessive Cu loading may reduce TiO_2 surface. In addition, Pt-doped TiO_2 nanoparticles have also been investigated and 0.13 wt% Pt/TiO_2 catalyst shows the maximum activity on CH_4 yield with 0.0565 mmol/ (gcat h) after 7h of UV irradiation [19]. The coupling of two semiconductors with unlike energy levels is helpful in achieving an efficient charge separation. Zhao et al explored the photocatalytic reduction of CO_2 to methanol, formic acid and formaldehyde when Co Pc/TiO_2 was the catalyst [20]. Adachi et al observed the use of Cu as a co-catalyst [21]. In his study, TiO_2 was dispersed in a CO_2 pressurized solution under the illumination of Xe lamp to give ethylene and methane. The methanol yield of 2.0 wt.% Cu/TiO_2 was 119 µ mol/g after 7 h of UV light radiation that was way higher than that of sol-gel TiO_2 and commercial TiO_2.

The size of the dopant also matters a lot in terms of increasing photocatalytic efficiency of TiO_2. It was observed that if Pt nanoparticle is too small, then quantum captivity effects cause the energy band separation to be too high for an excited electron to be transferred to the TiO_2. Contrariwise,

if the Pt nanoparticle is too big, it merely serves as a recombination center capturing both excited e^-- h^+, vastly reducing the efficiency of the system [22]. Thus, size of the metal dopant must be precisely controlled to enhance CO_2 reduction rates. Table 2.1 illustrates the various doped and undoped photocatalysts.

Nonmetal doping has also been initiated by researchers for TiO_2 photocatalytic reduction systems. The function desired from nonmetal doping is to extend the electromagnetic region. Thus, the photo catalyst is able to use the generate excited electrons by narrowing the bandgap of the photo catalyst system [23]. It allows for a greater portion of incoming light spectrum, thus, generating more *e*– - *h*+ pairs.

2.5.3. Other Semiconductor Systems

Current photocatalytic systems are not only constrained to TiO_2 but many other semiconductor systems like ZnO, MgO, GaP, SiC, WO_3 and various other metal oxides. Graphene oxide (GO) is also a promising material, though, effect of graphene on the product formation during the photocatalytic CO_2 reduction remains unclear. Graphene can efficiently reduce the electron−hole recombination rate in the semiconductor by functioning as an electron acceptor, thereby improving the photocatalytic CO_2 reduction activity [24]. Yiming et al prepared a ZnO/g-C_3N_4 composite photocatalyst by simple impreganation method that controlled and inhibited the recombination of electron–hole pairs [25]. ZnO/g-C_3N_4 photocatalyst proved to be an optimum CO_2 conversion nanomaterial with a rate of 45.6 mol h^{-1} g cat^{-1}, that was 6.4 and 4.9 times higher than P25 and G-C3N4, respectively. GaP was used as cathode in an electrochemical cell along with carbon anode and buffer electrolyte through which CO_2 was bubbled to give formaldehyde, methanol and formic acid [26]. CO_2 reduction into CH_4 in presence of water was done by WO_3 predominantly {002} facet [27]. Cd-rich CdSe nanocrystals are also efficient photocatalysts below a certain critical size on light incidence, while bulk CdSe surfaces are not [28]. Nanostructures in forms of nanowires, nanorods and nanotubes have been widely investigated for photocatalytic applications and proved to give superior performance. For instance, $Fe_2V_4O_{13}$ nanoribbons, $Na_2V_6O_{16}$ nanoribbon, ribbons, HNb_3O_8 nanoribbons, $NaNbO_3$ nanowires and $In_2Ge_2O_7$ hybrid sub-nanowires. Nanoribbons have an advantage of ultrathin geometry that greatly improved photocatalytic activity [29] [30] .

2.6. Synthesis routes for TiO_2

An exponential phase of research has been observed in synthesis of nanomaterials. Various chemical and physical techniques emerge to reduce the size of the materials smaller and smaller to nanometer range. This shrinkage in size makes changes in the properties of the synthesized nanomaterial. It increases the surface-to-volume ratio and surface area of nanostructure. But, the most important property to be effected is the electron hole recombination in the semiconductor nanostructures. The movement of electron hole properties largely depends upon the surface area and geometry of the nanomaterial. One such semiconductor dependent on such properties is TiO_2. TiO_2 is most affected by the size, arrangement and geometry of its building blocks.

Titanium dioxide exhibits three different polymorphs – namely anatase, rutile, and brookite [31]. With a mighty band gap of TiO_2, anatase and rutile polymorphs occupy at 3.2eV and 3.0eV respectively. Each polymorph originated from different ranges of the band gap and delivers different light responsive behavior. Since the capability of interaction with the light energy is the only quantifying parameter for the assessment of photocatalytic ability, tailor-made polymorph structures had been in high demand. Supporting this statement, various experimental evidence had been clearly reported the impact of acquired polymorph on the photocatalytic activity. These tailor-made structures of TiO_2 particles provide feasibility on controlling the morphology, crystalline phase, and particle size. It is clearly evident that these fundamental physical parameters have to be controlled during the process of manufacturing itself. But again, different synthesis methods deliver different physical properties, due to a variety of thermodynamic and chemical reactions undergone during the course of synthesis.

Various breakthroughs have been observed in the synthesis, modifications and its applications in various sectors in current years [33] [34]. There are numerous methods for the synthesis of TiO_2 nanomaterial such as sol-gel, hydrothermal. solvothermal, hydrolysis and water impregnation methods. All methods are versatile in their own ways with an ultimate of synthesizing modified TiO_2 nanoparticles. Table 2.2 illustrates the physical properties of TiO_2, synthesized via different methods.

Table 2.1: CO2 photo catalysis in the presence of doped/undoped TiO_2

S. No.	Light Source	Catalyst	Co-Catalyst	Reaction Medium	Products formation rate ($\mu molh^{-1}g\ cat^{-1}$)	Comments	Reference
TiO_2 nanoparticles							
1.	UV Hg lamp (254 nm)	TiO_2 nanoparticles (4.5 to 29 nm)		CO_2-bubbled NaOH solution	CH_4, CH_3OH	The optimum particle size was 14 nm.	[13]
2.	UV Hg lamp	TiO_2 nanoparticles	Cu	CO_2 and H_2O vapour	CH_3OH, CH4	Highest yield rates for the photo reduction of CO_2 were obtained when H_2 and water vapour were used in presence of UV light.	[14]
3.	UV lamp	TiO_2 nanoparticles		CO_2-bubbled NaOH solution	CH_3OH **(4.7)**	The methanol yield attained 250 μmol/g after 20 h of light illumination. Yield of methanol significantly increased by adding NaOH as indicated by experimental results.	[15]
		Degussa P25			CH_3OH **(38.2)**		
4.	UV lamp	TiO_2 nanoparticles	3.0 wt% CuO	CO_2-bubbled $KHCO_3$ aqueous solution	CH_3OH **(809)**	By the protonation of the intermediates in reaction, methanol was produced on the TiO_2 powders with CO_2 -bubbled $KHCO_3$ aqueous solution.	[16]
5.	75 W Hg lamp, 280 nm	TiO_2(100) nanoparticles		CO_2 and H_2O vapour	CH_3OH **(2.4)**	TiO_2 (100) phase performed a higher the production rate of methanol than TiO_2 (110).	[17]

		TiO_2(110) nanoparticles			CH_3OH **(0.8)**		
6.	150 W solar simulator	TiO_2 (anatase)		CO_2 and H_2O	CH_4 **(0.19)**		[18]
7.	UV lamp (254 nm)	TiO_2		CO_2-bubbled NaOH solution containing Na_2SO_3	CH_3OH **(17.3)**	A composite of TiO_2 particle with 89% anatase and 11 % rutile was used. Yield at 365 nm and 400-780 nm was 3.6 and 1.1 respectively.	[19]
8.	UV Hg lamp (365 nm)	TiO_2		CO_2 and H_2O vapour	CH_3OH **(0.06)**	The methanol yield increased with UV intensity. Various other parameters like pressure, light distance etc in reactor were optimised.	[32]
TiO2 nanoparticles doped with some metal							
9.	UV lamp (365nm)	Cu, co-doped TiO_2 nanoparticles	Mn codoped	CO_2-bubbled NaOH Solution	CH_3OH	With the increase in loading amount of Cu, Unfortunately, the activity was lowered and the primary product was converted from CO to CH_4.	[20]
10.	UV lamp	TiO_2 nanoparticles	2.0 wt% Cu	CO_2-bubbled NaOH solution	CH_3OH **(118)**	The photocatalytic activity reached maximum on the outer most surface of a TiO_2 particle where 25% of the total Cu loading was located.	[21]
11.	UV lamp (254 nm)	N co-doped TiO_2 nanoparticles	4.0 %	CO_2-bubbled NaOH solution containing Na_2SO_3	CH_3OH **(245.4)**	The CO_2 reduction efficiency of TiO_2 film was better with one-layer Ni-doped than the multi N-doped layers TiO_2 film when exposed to UV light. N-Ni/TiO_2 was most suitable for the photoreduction of CO_2 and gave highest methanol yield in the same condition.	[22]
		Ni co-doped TiO_2 Nanoparticles	6.0 %		CH_3OH **(214.4)**		
		N-Ni co-doped TiO_2 nanoparticles	4 % N and 6% Ni		CH_3OH **(482.0)**		

12.	UV Hg lamp (365 nm)	TiO_2 coated on optical fiber	1.2 wt % Cu	CO_2 and H_2O vapour	CH_3OH **(0.45)**	Methanol production increased with UV light intensity. Photo activity was found to be increased with increasing Cu amount.	[32]
13.	8W Hg lamp (254 nm)	Cu-TiO_2	2.0 wt % Cu	0.2N NaOH solution	CH_3OH **(1000)**	By adding $CuCl_2$, the methanol yield considerably increased. The activity of the catalysts followed the order $CuCl_2$-1 h ~ $CuCl_2$-3 h > $CuCl_2$-0 h > $CuAc_2$-8 h > $CuCl_2$-8 h.	[23]
		Ag-TiO_2	2.0 wt.% Ag		CH_3OH **(300)**		
14.	15 W UV lamp (365 nm)	Ni-TiO_2	6 wt % Ni	0.2 mol/l NaOH and 0.2 mol/l Na_2SO_3	CH_3OH **(7.51)**	Improved photoactivity of the doped photo catalysts compared to pure TiO_2 was due to Ni^{2+} acting as an electron trap, thus facilitating enhanced charge separation.	[24]
	Incandescent lamp (400-780 nm)	Ni-TiO_2	6 wt % Ni	CO_2 and H_2O vapour	CH_3OH **(3.59)**		[25]
15.	UV lam	CuO/TiO_2 nanoparticles	3.0 wt% CuO	CO_2-bubbled $KHCO_3$ aqueous solution	CH_3OH **(2655)**	TiO_2 nanoparticles with CO_2-bubbled $KHCO_3$ aqueous solution produced methanol by the protonation and reduction of the reaction intermediates on the. Various CuO concentrations used were 0.5 %, 1.0 %, 5.0 %, 10.0 % and 3.0 % Cu_2O. Optimum concentration was 3.0 wt % CuO.	[26]

Table 2.2: Various synthesis routes for TiO2 nanomaterial

S.No	Raw materials	Synthesis route	Acids used / pH/ molarity		Polymorph	Morphology	Size (nm)	Comments & References
1.	7ml of 0.063 M of $TiCl_4$ dissolved in 150ml of .001M PEG	Sol gel method	No acids used	pH 3 & pH 5	Rutile phase	Spherical	100	pH optimization was done with ammonia solution. Rutile phase existed at lower pH and anatase phase at higher pH. [13]
				pH 7	Mixture of anatase & rutile phases	Agglomeration and irregular shape	200	
				pH 10	Anatase phase	Agglomeration and few rod-shaped		
2.	Titanium(IV) isopropoxide (97%) dissolved in isopropyl alcohol (95 % solution)	Sol-gel method	No acids used	pH 1	Rutile phase	Rod-shaped	13.6	pH optimization by NH_3 for acidic condition and NaOH for the basic condition. Rutile phase existed at lower pH and anatase phase at higher pH. [22]
				pH 3 & pH5	Anatase phase	Spherical	8.2, 7.9	
				pH 7	Anatase phase	Agglomerated	9	
				pH 9	Anatase phase	Agglomerated	8.4	
3.	Titanium isopropoxide dissolved in ethanol solution & added dropwise against HCl	Sol-gel method followed by hydrothermal treatment	HCl	pH < 1	85% anatase & 15% brookite	Spherical	-	At smaller particles size and higher pH, anatase particles are stable. [25]
				pH 1-2	Part of anatase transformation to rutile		Avg. size 3.4	
				pH > 6	Part of anatase transformation to brookite		3-4	
				pH > 12	Part of anatase remained unchanged		3.5	
4.			HCl	> 1M	Pure rutile phase		20	

	3.4 ml of Tetra butyl titanate dissolved in 4ml of 5M HCl	Hydrothermal method		< 1M	Mixture of anatase & rutile	Needle-like particles		Higher concentration of HCl favours the formation of rutile phase. [11]
5.	Fusion of rutile mineral and NaOH at (1:2) & dissolved in different molarities of HCl	Hydrolysis	HCl	0.5M	74% Rutile & 26% anatase	Spherical morphology on primary particles or crystallites	11.97	With increase in molarity, crystallite size decreases. [17]
				1M	79% Rutile & 21% anatase		11.32	
				2M	100% rutile		8.9	
				3M	100% rutile		6.7	
				4M	100% rutile		6.7	
				<1M	Mixture of anatase & rutile		4.3	
6.	2.4g of TiOSO4 mixed with 25ml of H2O. 25ml of CTAB (60mM) as the template material. On different HCl (0.1 to 8M) conc. the reaction had been carried out	Hydrothermal method	HCl	0.1M - 1M	Pure anatase phase	Aggregated irregular shaped nanoparticles	13 – 15	Rutile phase dominates the anatase in 1-5M HCl based precursor mixture. The maximum rutile phase had evolved at 5M HCl based precursor mixture. Then the anatase was prominent at 5-8M HCl based precursor mixture. [27]
				2M – 7M	Mixture of anatase & rutile		9	
				5M – 8M	Proportion of Anatase phase increases		14.5	
				8M	Pure anatase phase			
7.	A stock solution of 5.27M of $TiCl_4$ dissolved in HCl.	Hydrolysis	HCl	1.5M – 3.8M	Mixture of rutile & brookite	Rod-shaped agglomerates	20 – 50	With the increase in HCl conc. rutile phase decreased. When reaction time increases brookite forms. Brookite increases up to 15h but its formation decreased after that. Rutile formed after 25 h. [29]
				4.5M – 6.5M	Mixture of rutile & brookite	Square and spherical particles	5 – 20	
				8M	Rutile phase	Long spindle shaped	20	
8.	$TiCl_4$ dissolved in HNO_3	Hydrolysis	HNO_3	0.5 M- 2M	Major - Anatase & Secondary brookite	Spherical	5-50	$TiCl_4$ dissolves better in HCl than HNO_3. The reaction products of the

								hydrolysis are highly complex, under HNO_3 medium. Thus, brookite formation and existence had been suppressed at lower pH itself. [33]
9.	$TiCl_4$ dissolved in HNO_3	Hydrolysis	HNO_3	0.5 M-2M	Major - Anatase & Secondary brookite	Spherical	5-50	$TiCl_4$ dissolves better in HCl than HNO_3. The reaction products of the hydrolysis are highly complex, under HNO_3 medium. Thus, brookite formation and existence had been suppressed at lower pH itself. [33]

Two synthesis methods reported for TiO_2 nanoparticles are gas phase and liquid phase method. The gas phase method is quiet difficult and consumes high energy, though the prepared TiO_2 has a high mono dispersity, a great purity, and comparatively small size [35]. The hydrolysis, hydrothermal, micro emulsion, sol-gel, and magnetic deposition are the most commonly used liquid phase methods. Among these methods, hydrolysis method had been considered to be the simplest method, which can be carried out in laboratory conditions itself. In this method, the titanium source, in the form of a liquid precursor, this tends to undergo hydrolysis to form Titanium hydroxide. On further treatments, the titanium hydroxide transforms to titanium oxide particles. The liquid precursor used, which had been calculated in the molecular level, leads to attaining titanium dioxide particles with high purity.

In the hydrolysis method, the processing parameters, such as precursor concentration, the volume of precursor mixture, pH, and atmospheric conditions have a great influence on the purity, phase formation and particle size of the particles. It had been observed that highly acidic conditions of the precursor mixture would form rutile crystalline phase, whereas anatase polymorph had been evolved at higher pH conditions. Due to higher surface energy of the particles, severe agglomeration, and higher particle size had been attained at base pH conditions [36]. Furthermore, pH of the precursor mixture has a major influence in the degree of crystallinity. The acidic conditions of the precursor mixture promote crystallinity and achieve bigger crystallite size particles [37]. In order to initiate and accelerate hydrolysis rate of the titanium source, the acid catalyst had been used. The ratio between the concentration of the acid catalyst and concentration of titanium ions decides the crystalline phase of the end product. In the case of HCl, as an acid catalyst, it had been observed that higher concentration of the acid suppresses the rutile crystalline phase and reduces the ultimate crystallite size of the TiO_2 particles [38] [39].

[40] investigated that activation energy plays a crucial role in transformation of one phase to another. Interfacial tension and surface charge change with pH in an aqueous solution. This in turn changes the phase stability. At pH values, below the point of zero charge (pHzpc) of titania (3-6), rutile particles are more stable while anatase particles are more stable when pH is above pHzpc. In addition, it has been suggested that pZC shifts to a lower pH and particle size increase of anatase spheres and rutile rods [41].

Molarity also plays a crucial part in the phase formation of TiO_2. Wu et al observed that with the decrease in concentration of HCl below 1M, mixture of anatase and rutile were formed with a needle morphology of rutile particles [42]. Only rutile phase was observed when acid molarities was high and anatase phase was not detected. Dilute acid produced spherical rutile particles with largest crystallite size [43].Thus, the synthesis conditions and factors such as the crystalline structure, morphology of the surface and stability of the phase should be optimized. Optimizing these parameters will result in formation of high purity TiO_2 nanoparticles.

Chapter 3

Materials and Methods

3.1. Chemicals used

Titanium tetrachloride (99.9%, trace metal basis), Titanium (IV) isopropoxide (99.9 % trace metal basis), P25 (commercial TiO_2) and Niobium (V) oxide was procured from Sigma Aldrich. Hydrochloric acid (35% purity) was purchased from Loba Chemie, India. Various solvents like methanol and acetone (L.R) were procured from HiMedia Laboratories. All other chemicals employed in the experimentations were of Analytical Grade (AR) procured from HiMedia Laboratories.

3.2. Preparation of various catalysts

3.2.1. Preparation of TiO_2 by hydrolysis method

Titanium oxide solutions were obtained by hydrolysis method. This process formed an amorphous solid which is further transformed to crystalline form by aging or heat treatment. In the present work, TiO2 powder was prepared by modifying the synthesis proposed by (Wenjun Zheng, 2009) who used titanium tetrachloride into hydrochloric acid. For the preparation of the solution, 1 ml of pure titanium tetrachloride was added slowly dropwise to various volume of hydrochloric acid that range from 50 mL to 200 mL at room temperature which was kept for stirring at 250 rpm for 12 hours to yield a homogeneous solution. Thereafter, the formed solutions were kept for heating and aged at 100 °C for 12 h to 15 h in an oven to evaporate acid. The product was isolated by centrifugation done at 7000 rpm by washing with deionised water and anhydrous ethanol for 15-20 times. After washing, product was calcined at 450°C for 6 hours. Hydrochloric acid aided as an acidic catalyst in order to monitor the hydrolysis rate of source of titanium whose concentration was varied from 1 $mol \cdot dm^{-3}$ to 3 $mol \cdot dm^{-3}$ while volume varied form 50 ml to 200 ml. By altering the concentration and volume of hydrochloric acid ratio of rutile to anatase could be optimised. The hydrolysis reaction that lead to the formation of TiO_2 is given by the following reactions (1, 2 and 3):

$$\mathbf{TiCl_4 + HCl + 2H_2O \xrightarrow{Hydrolysis} TiO_2 + 5HCl} \qquad \mathbf{(1)}$$

$$2\,TiO_2 + 5\,HCl + C_2H_5OH \xrightarrow{\text{Washing}} TiO_2 + TiOH + 3H_2O \quad (2)$$

$$TiO_2 + TiOH + 5\,HCl + H_2O \xrightarrow{\text{Drying}} TiO_2 \quad (3)$$

3.2.2. Preparation of TiO_2 catalyst by sol-gel method

Titanium isopropoxide (2ml) was dissolved in 5 ml of freshly dried methanol under constant stirring. 5 ml of deionized water was slowly dripped into the solution and stirred for half an hour. Solution was then kept for aging for 24 hours at room temperature followed by washing foe several times by deionized water and anhydrous ethanol. Subsequently, powdered and kept for calcination at 450°C in air for 5 hours resulting in the formation of TiO_2 nanoparticles.

3.2.3. Preparation of Nb loaded TiO_2 catalyst

Niobium doped Titanium dioxide nanoparticles were synthesized by sol-gel route. Niobium pentaoxide (Nb_2O_5) and titanium isopropoxide [TTIP] were employed as a precursor for niobium and titanium dioxide respectively. Two different concentrations, 0.04 M and .08 M of Nb were used for the synthesis of composite. 20 mg and 40 mg of niobium salt was mixed with 5 ml of methanol 0.04 M and 0.08 M concentration of Niobium. After a few minutes, 30 mg of sodium borate ($NaBH_4$) was added to the same 5 ml methanol to reduce the metal ions. Polyethylene glycol solution was prepared when 200 mg of PEG was added in 5 ml of methanol. Finally, titania supported catalysts (1 wt.%) were prepared by adding water to the above prepared solution with continuous stirring for 15 minutes. 2.02mL of TTIP was mixed in 5mL of freshly dried methanol and then, slowly added to the solution. Within 15–20 seconds, a gel formation occurred and kept for overnight aging. This was followed by drying at a temperature of 150°C for 2h. The dried gel was made into powder and later on, calcined at a temperature of 425°C for 4 h.

3.3. Characterization of nanomaterial

3.3.1. X-Ray Diffraction Studies (XRD)

XRD measurements were performed on RIGAKU Japan/Ultima IV XRD system using Cu Kα Radiation (λ = 1.5418 °A) with the scan range of 2θ = 5-90 ° at a speed of 20 °/min. Phase identification was carried out by matching the observed XRD pattern with the expected pattern available from Joint Committee on Powder Diffraction Standards (JCPDS). The crystallite size of the catalyst samples were calculated by the Scherrer's formula [44].

$$\mathbf{t = \frac{K*\lambda}{\beta*Cos\ \theta}} \quad \textbf{(4)}$$

where t → crystallite size

K → constant dependent on crystallite shape (0.9)

λ → X-ray wavelength (1.54056 °A)

β → FWHM (full width at half maximum)

θ → Bragg's angle

The relative phase percentages of TiO_2 can be expressed as a function of XRD peak areas of different phases (anatase and rutile), based on the following equation [45]:

$$\mathbf{W_A = K_A I_A (K_A I_A + I_R)} \quad \textbf{(5)}$$

$$\mathbf{W_R = I_R / (K_A I_A + I_R)} \quad \textbf{(6)}$$

where W_A and W_R are the weight fraction of anatase and rutile and I_A and I_R are obtained from characteristic peaks areas of anatase and rutile respectively with $K_A = 0.886$ as constant.

3.3.2 Field Emission Scanning Electron Microscopy Studies (FESEM)

The morphology and size of the particle was investigated under a Nova Nanosem 450 FESEM. The samples were prepared by sonicating TiO_2 powder in acetone at a frequency of 20 KHz and 100 % amplitude for 15 minutes.

3.3.3. Transmission electron microscope

Transmission electron micrographs were recorded using Bruker Nano GMBH (Germany) at 200 kV. 1-2 mg of the powder was sonicated in 5 mL of ethanol and dispersed well by ultra-sonicating for 15 minutes and a small drop of the dispersed solution was added on a carbon coated copper grid and kept for drying at room temperature. Morphology and composition was studied in depth by this instrument.

3.3.4. Thermogravimetric Analysis (TGA)

Weight loss studies were done by TGA to assure proper washing and removal of all trace elements. Samples were analysed from 25 °C to 650 °C using a DSC/TGA analyser (Netzsch, Germany, STA449C/4/MFC/G) with a heating rate of 10 °/min under controlled argon atmosphere.

3.3.5. Fourier Transform Infrared Spectroscopy (FTIR)

Study of molecular bonds in the material was done by FTIR. The transmission spectra were analyzed on a Shimadzu, IR prestige-21. A mixture of powdered samples and Potassium Bromide (KBr) were pressed together to form pellets.

3.3.6. Photoluminescence analysis

Photoluminence (PL) spectroscopy of nanomaterials was done by Horiba Jobin Yvon, USA/Fluoromax 4P. It is used for investigating energy level and information on emission and excitation spectra of a photocatalyst. The PL spectra of titania samples was in the wavelength region of 250-700 nm with excitation at 200 nm.

3.3.6. UV-Visible spectrophotometer

UV-Visible diffuse reflectance spectra were obtained to investigate the light absorption characteristics of TiO_2 nanoparticles. The spectra were recorded at 25 °C in presence of air from 250 to 700 nm. The band gap of the samples was calculated by Kubelka-Munk Plot:

$$\mathbf{F\,(R)} = \frac{\mathbf{k}}{\mathbf{s}} = \frac{\mathbf{(1-R)^2}}{\mathbf{2R}} \qquad \textbf{(7)}$$

where R is reflectance, F(R) is Kubelka-Munk Function

3.4. Reaction conditions for photoreduction of CO_2

An initial set up of photo reactor at laboratory scale was constructed having a 15 W UV lamp along with a balloon bubbling CO_2 monitored by a pump and a reaction medium loaded with photocatalyst. 400 ml of 0.2 N NaOH was used as a reaction medium in which 0.1 g of catalyst was added. CO_2 was bubbled for 2 h 40 mins approx. Figure 3.1. describes the complete laboratory setup. Blank experiments were carried out to confirm that the product formation was because of the photo reduction of CO_2.

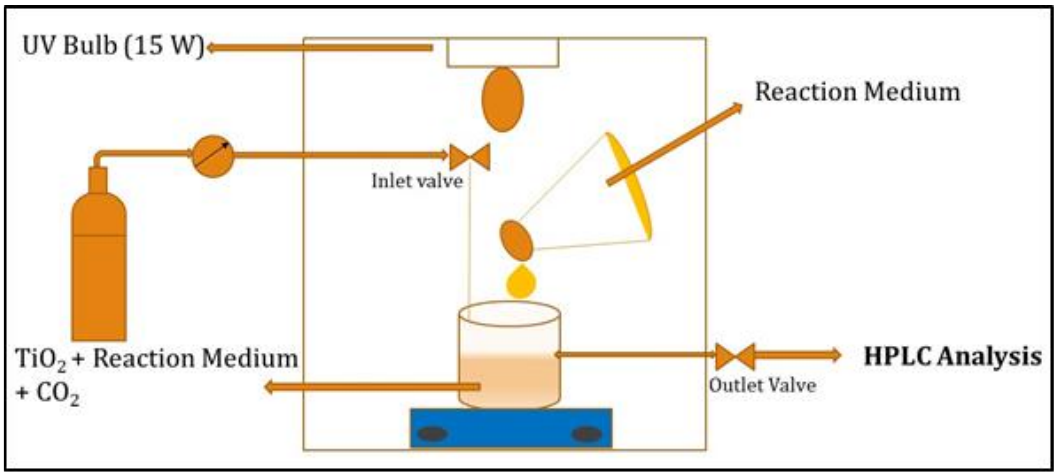

Figure 3.1: Laboratory set up for photocatalytic reduction of CO_2

The products were examined by High Performance Liquid Chromatography (HPLC). HPLC was a Shimadzu make armed with refractive index detector and Agilent Hiplex Hl-17 column. Samples were injected using a 20 µl Hamilton loop. 0.1 % Methanol (Sigma, HPLC grade, 100 % purity) was used as standard. Peak identification was on the basis of HPLC retention times when compared with that of standard. The analysis was performed at 60°C with a flow rate of 0.7 ml/min using 5mM H_2SO_4 as a mobile phase. Prior to the analysis, the eluent was filtered with 0.22-µm nylon GV membrane.

External standard Quantitation method was used to calculate the amount of analyte. It is the basic quantitation procedure in which both standard and unknown samples are analysed under the same conditions. It uses absolute response factors. The response factor is normally calculated as amount/area of analyte in the caliberation sample. In subsequent saamples, amount of individual component is calculated by applying the response factor to the measured sample area. Equations 1 and 2 were used to calculate amount of analyte.

Calculations:

$$\textbf{Response factor} = \frac{\textbf{Peak area}}{\textbf{Standard Amount}} \qquad \textbf{(8)}$$

$$\textbf{Amount of analyte} = \frac{\textbf{Peak Area}}{\textbf{Response Factor}} \qquad \textbf{(9)}$$

Chapter 4

Results and Discussion

4.1. Yield of nanoparticles

1ml of $TiCl_4$ had been hydrolyzed against 50, 100, 150 and 200ml of 1M, 2M and 3M HCl solution. After washing with series of concentrations of ethanol and water, the yield of Titanium dioxide nanoparticles had been weighed and given in Table 4.1. It had been found that the yield of Titanium dioxide nanoparticles had been decreasing gradually with higher volumes of HCl. Since the nucleation rate will be vigorous, and particle interaction is high in lower volumes of the aqueous solutions, the yield of titanium nanoparticles had been obtained with a higher amount. With the increase in concentration from 1M to 3M, yield was found to be increased.

Table 4.1: Yield of Titanium dioxide nanoparticles by hydrolysis method

Sample	Volume of Solution	TiO_2 powder yields before washing (in grams)	TiO_2 powder yields after washing (in grams)
1 mol.dm^{-3}			
S1	50 mL	0.775	0.734
S2	100 mL	0.72	0.604
S3	150 mL	0.54	0.49
S4	200 mL	0.31	0.231
2 mol.dm^{-3}			
S5	50 mL	0.779	0.669
S6	100 mL	1.01	0.606
S7	150 mL	0.88	0.49
S8	200 mL	0.829	1.997
3 mol.dm^{-3}			
S9	50 mL	0.881	0.765
S10	100 mL	0.779	0.589
S11	150 mL	1.025	0.516
S12	200 mL	0.779	0.609

Monometallic Nb doped TiO_2 nanoparticles were synthesized successfully using $NaBH_4$ as reducing agent. The Nb particles were entrapped in titania nanoparticles surface through sol-gel method. The final filtrate was colorless over the gel, henceforth, indicates that Nb particles were

fully dispersed on the titania surface. Yield of Nb-doped TiO_2 composite increased with the increasing concentration of dopant. It was 0.62 g and 0.76 g for 0.04 M and 0.08 M concentration of Nb.

4.2. Characterization of nanoparticles

4.2.1. XRD studies

The crystalline phases obtained from the above mentioned samples had been determined by XRD technique. The obtained phases on the synthesized Titanium dioxide nanoparticles had been shown in the Figure. 4.1. The synthesized titanium dioxide nanoparticles attain neither a pure anatase phase nor a pure rutile phase. The obtained phases are a combination of rutile and anatase phases. The rutile polymorph is reduced with increase in volume of 1mol.dm^{-3} to 3 mol.dm^{-3} HCl. Since the synthesized titanium nanoparticles featured with binary phase of anatase and rutile, the weight fractions of the individual had been evaluated by using Eq.1 and Eq.2, which had been reported in the Table 4.2. The peaks are quite wide indicating incomplete crystallization because it has amorphous component. This result of TiO_2 sample is a universally accepted feature of nanoparticles [44].

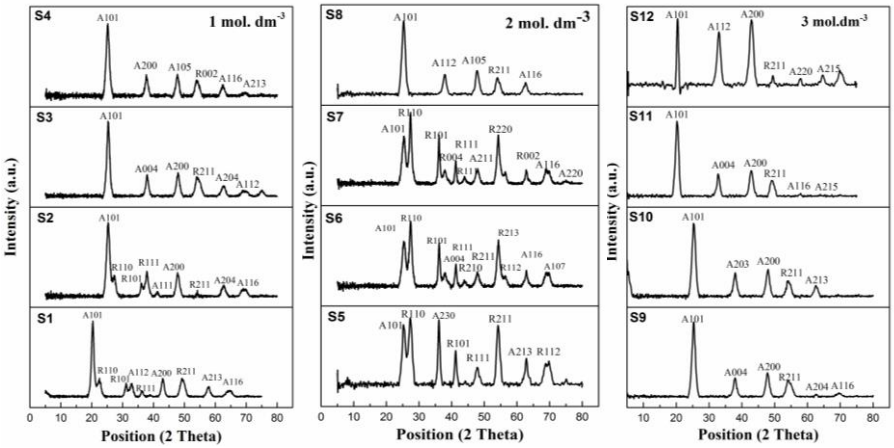

Figure 4.1: Phase Analysis of Titanium dioxide nanoparticles

It has been reported that with an increase in concentration of HCl anatase phase formation would increase [45]. From the XRD studies, a similar trend for volume as well as concentration of HCl was observed. pH of the medium also has vital effect on phase formation of TiO_2 nanoparticles. Anatase phase is dominant in highly acidic medium which is conflicting to partial charge model [46]. According to the concept of partial charge model, it is found that highly acidic medium solution favors rutile phase. This is due to the hydrolysis of titanium cation to form a stable specie

$[Ti(OH)(OH_2)_5]^{3+}$ which is further deprotonated to $[Ti(OH)_2(OH_2)_5]^{2+}$. These species condensed to form rutile and anatase phase by oxolation and deoxolation of further protonated species. In lower pH range, oxolation between linear chains leads to rutile formation, though, deoxolation did not happen. The stabilization of anatase at a high pH and of rutile at a low pH is in consistent with reports of numerous prior studies [47] [48] [49]. Nevertheless, the model predictions of phase stability of above literature reports are inconsistent with our results.

Table 4.2: Phase evaluation of synthesized Titanium dioxide nanoparticles

Sample	Crystallite size (nm)	JCPDS Rutile file	JCPDS Anatase file	Anatase %	Rutile %
S1	10.3	01-1292	01-0562	59.0	40.9
S2	5.0	01-1292	01-0562	68.6	34.6
S3	10.9	02-0494	01-0562	71.9	27.7
S4	5.7	02-0494	02-0387	71.9	26.7
S5	14.1	01-1292	02-0387	54.6	45.3
S6	13.8	01-1292	02-0406	53.6	46.9
S7	16.7	02-0494	02-0387	50.0	50.0
S8	8.2	01-1292	01-1167	75.3	24.3
S9	46.2	77-0440	71-1167	75.6	24.3
S10	51.3	76-0326	01-0562	72.4	27.5
S11	52.9	78-1508	75-1537	72.6	27.3
S12	53.3	76-0138	71-1167	67.4	32.5

When doped with niobium, XRD diffraction peaks of TiO_2 shifted towards lower theta values and diffraction angles. This might be attributed to the replacement of smaller Ti with larger Niobium ions in Nb-doped TiO_2, thus, resulting in small TiO_2 lattice expansion. This can be illustrated in Figure 4.2. The nanoparticles were crystalline in nature and the peaks were corresponding to the anatase [101] phase (JCPDS file no. 71-1166). Table 4.3. gives the details of the crystallite size of the synthesized nanomaterial. The crystallite size is in full accordance with the TEM analysis explained in the later part. No characteristic peaks for Nb or NbO_2 were found in the XRD diffraction patterns. Thus, it can be understood that the Nb amount was quiet low, which resulted in absence of the Nb peaks and complete dispersion of Nb ions on TiO_2 lattice [50].

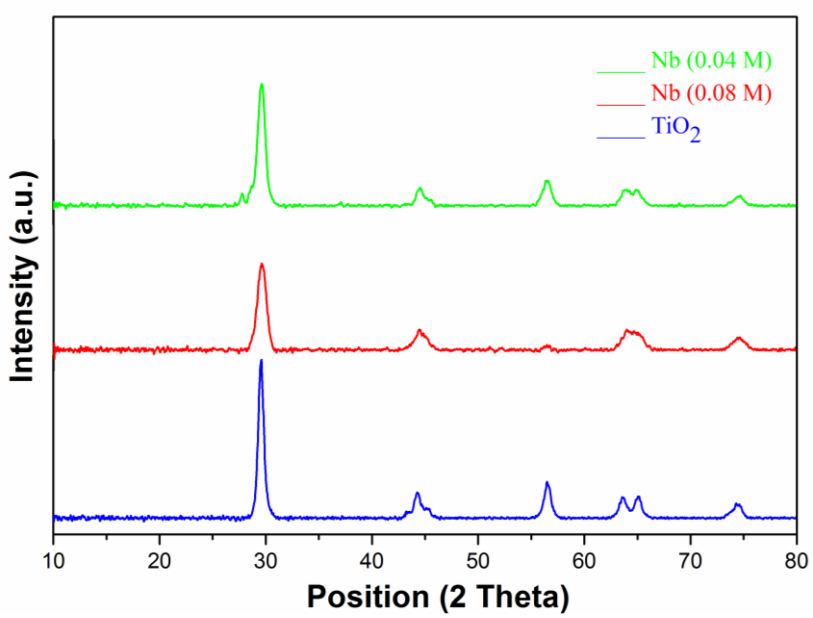

Figure 4.2: XRD pattern of Nb-doped TiO_2 and sol-gel TiO_2

Table 4.3: The crystallite size of TiO_2 and Nb-doped TiO_2 nanoparticles

Sample	Crystallite size (nm)
TiO_2	8.5
Nb-doped TiO_2 (0.04 M)	7
Nb-doped TiO_2 (0.08 M)	6.8

4.2.2 FESEM studies

The microstructures of titanium dioxide nanoparticles and its composite with Niobium had been illustrated in the Figure 4.3 and 4.4. All the samples synthesized by hydrolysis method acquired particle size in the range of 20nm to 90nm. It clearly shows that the samples S1, S2 & S4 attained a cubical morphology. But the morphology of S3 was partly spherical and partly cubical. This clearly shows an unstable structure which had been attained due to the transformation of phase from rutile to anatase. At lower pH or acidic medium, particles are little agglomerated that is corraborated with the results of Devi, et al [36]. The similar kind of profile had been clearly illustrated in the results of phase analysis.

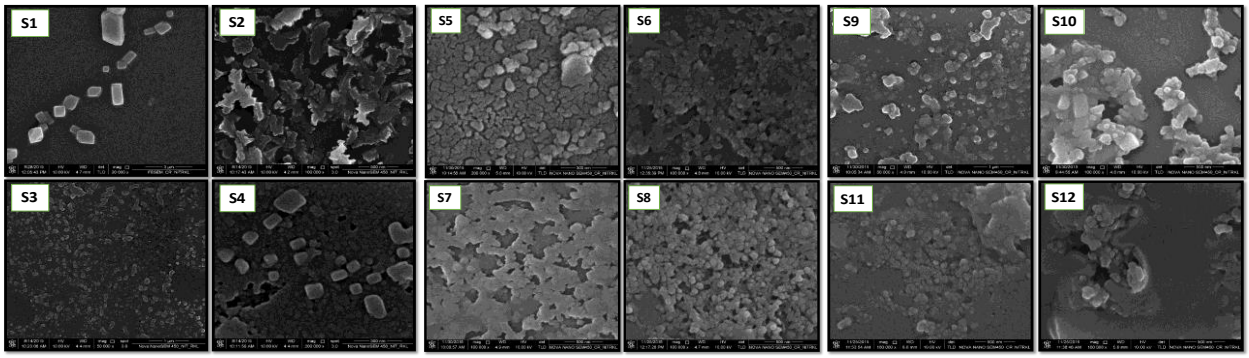

Figure 4.3: FESEM images of Titanium dioxide nanoparticles synthesized by hydrolysis method

In case of sol-gel TiO_2, the surface of nanoparticles was smooth and had regular spherical morphology. However, Nb doping induced morphological changes and size reduction in the nanomaterial. Many small particles with rough surface were found on the surface of titania. The deposited particles were also spherical in nature and had a size distribution centering from 30 nm to 60 nm. The sol-gel TiO_2 and Nb- doped TiO_2 ranged from 30 nm to 60 nm than the commercial P25 powder size that ranged from 90 nm to 110 nm. This truly complies with the investigations of [51].

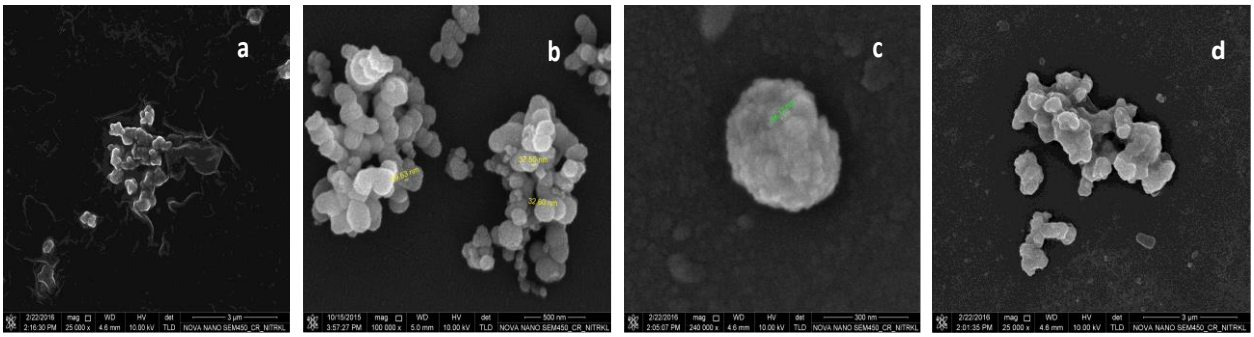

Figure 4.4: FESEM image of a) P25 b) TiO_2 c) and d) Nb-doped TiO_2

4.2.3. TEM Studies

TEM, high resolution TEM (HRTEM) and selected area diffraction (SAED) analysis confirm the size and changes in the morphology of TiO_2 nanomaterial after doping with Nb. More accurate measurement and intense structure could be revealed by this technique. It showed that the distribution of Nb in TiO_2 was non-uniform. Nb metal was incorporated partly in TiO_2 lattice that might promote anatase phase formation in TiO_2 [52]. Nb^{4+} has a larger ionic radius (0.65 A°) than Ti^{4+} (0.60 A°). This property enabled Niobium to diffuse into the lattice of TiO_2 and replace Ti^{4+} ions. With the increase in concentration of Nb, size of the particles increased from the range of 10

nm to 20 nm. [53] investigated with the increase of concentration of Nb, size of the particles increased. Similarly, nanomaterial increased in size of from 10 nm to 20 nm when concentration of Nb was increased from 0.04 M to 0.08 M. Figure 4.5 and 4.6 illustrates the TEM/ HRTEM, line scan and SAED images with different magnification. The Nb-doped TiO_2 samples were highly crystalline as proved from the SAED patterns. Though, crystallinity of the composites increased from lower niobium concentration 0.04 M to higher niobium concentration 0.08 M.

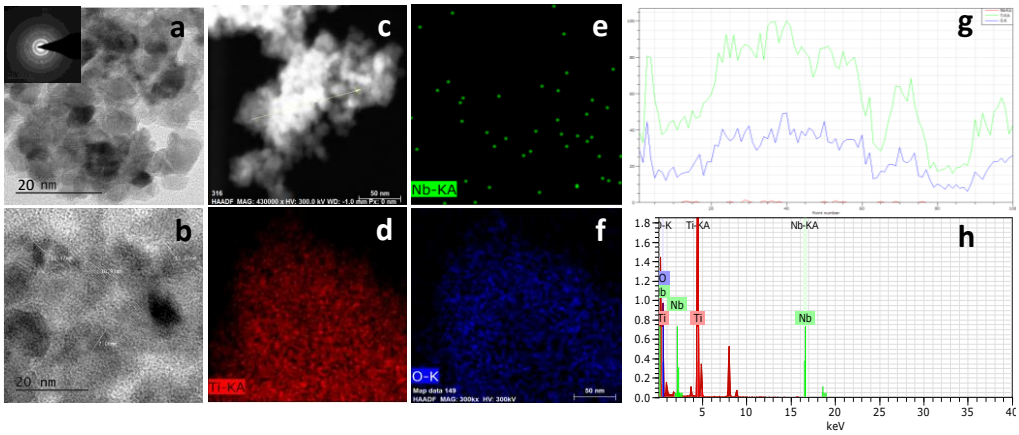

Figure 4.5: a) TEM image of 0.04 M Nb-doped TiO_2 b) HRTEM image d) The equivalent elemental mapping of Ti e) Nb and f) O g) Line scanning indicated by a line. The inset shows the SAED pattern

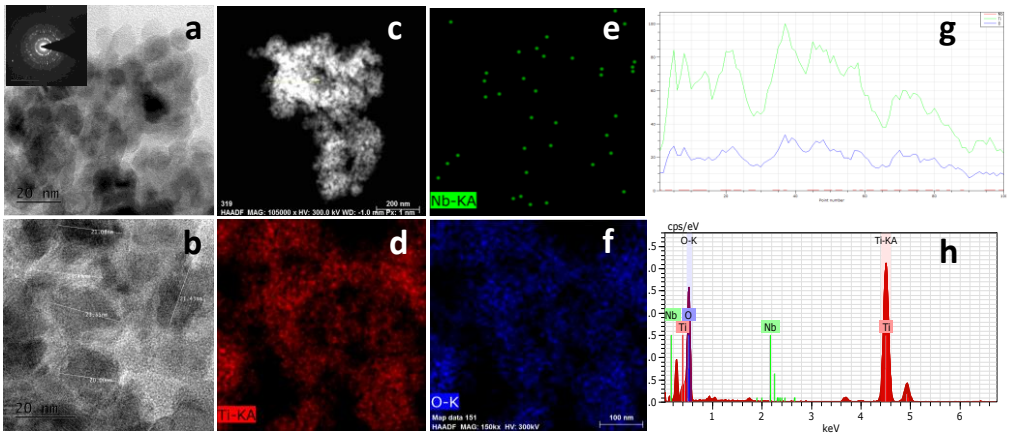

Figure 4.6: a) TEM image of 0.08 M Nb-doped TiO_2 b) HRTEM image d) The equivalent elemental mapping of Ti e) Nb and f) O g) Line scanning indicated by a line. The inset shows the SAED pattern

4.2.3. Weight loss studies by TGA

The thermogravimetric analysis of the samples with various concentrations and volumes are illustrated in the Figure 4.7. For the samples with constant volume as 50 ml, weight loss of around 12%, 18% and 17% respectively for 1 $mol.dm^{-3}$, 2 $mol.dm^{-3}$ and 3 $mol.dm^{-3}$ was noticed when the temperature reaches to 400°C. Similarly, for constant volume of 100 ml weight loss of around 16

%, 12% and 7 % respectively for 1 mol.dm^{-3}, 2 mol.dm^{-3} and 3 mol.dm^{-3} had been observed. These weight losses might be due to the evaporation of water, HCl and decomposition of unreacted Ti-OH molecules [54]. On further heat treatment, the unreacted Ti-OH molecules decompose to form TiO_2. Thus, if the samples had been heat treated, the weight fractions of anatase and rutile might change due to phase transformation and simultaneous crystallization.

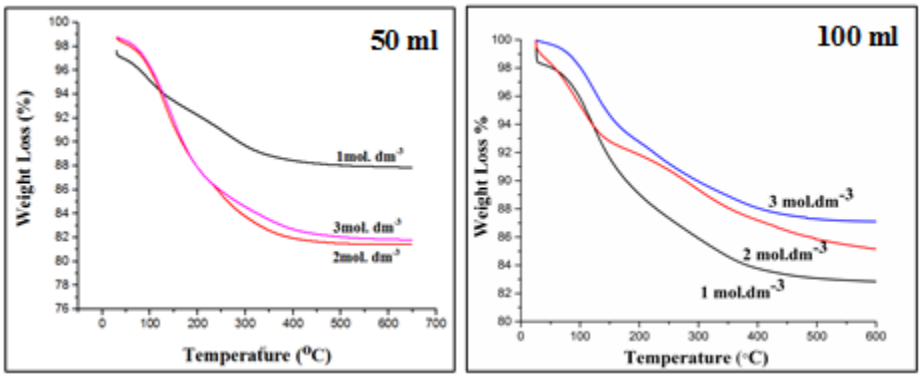

Figure 4.7: TGA analysis of Titanium dioxide nanoparticles for 50 ml volume of HCl with varying concentration from 1M to 3M

4.2.4. Chemical bonding analysis by FTIR

FTIR spectrometer was done to study the chemical bonding of TiO_2. Figure 4.8 illustrates the FTIR peaks of the photocatalysts. Peak centered at 3400 cm^{-1} might be ascribed to the presence of H_2O molecule. The band at 1630 cm^{-1} could be due to the presence of bending vibration of H-O-H bond [55]. The intense and broad peak in the range of 450-700 cm^{-1} might be due to the Ti-O bonds. The stretching vibration at 600 cm^{-1} is due to the presence of Nb-O bond. A broadening of band was observed that might be due to the existence of Nb content [56]. The bands at 3421 cm-1 and 1627 cm-1 are due to the stretching vibration of –OH group. The deformation around 1640 cm^{-1} is due to H-O-H bond and doped niobium in the structure. Moreover, the peak shifting in the range of 1200 cm^{-1} to 1700 cm^{-1} corroborate the replacement of Ti sites in TiO_2 lattice with Nb [57].

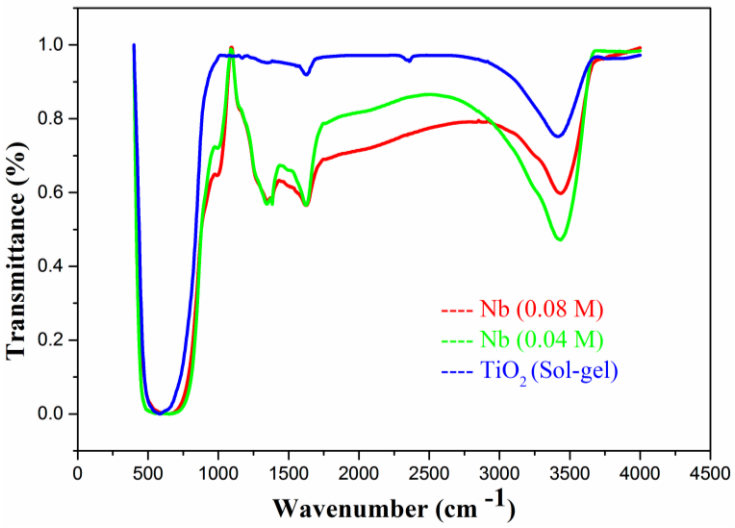

Figure 4.8: FTIR study of Nb-doped composite

4.2.5. Photoluminence analysis

Photoluminence (PL) spectroscopy of nanomaterials was done by Fluorescence Spectrometer. It is used for investigating energy level and information on emission and excitation spectra of a photocatalyst. The PL spectra of titania samples was in the wavelength region of 250-700 nm with excitation at 200 nm. For samples with 1M HCl and varied volume from 50-200 ml, PL intensity increased with increase in volume. This can be due to increase od titanium ions in the solution that effects crystal structure and ultimately band gap. At lower PL intensity, there will be a delay in rcombination rate, thus, higher photocatalytic activity. Hence, samples with lower volume have higher photocatalytic activity. Crystallite size increases with volume, thus more oxygen defects and more PL intensity. Similar was the scenario with 2M and 3M. Figure 4.9 (a, b, c) depicts the trend of PL spectra in 1M, 2M and 3M TiO_2 samples.

Several investigations reported the consequence of deposition of metals on TiO_2 in terms of PL intensity that had an impact on the photocatalytic activity of the semiconductor. When niobium was deposited on surface of TiO_2, the PL intensity decreased tremendously with respect to undoped TiO_2. This indicates that doping with a metal effectively hinders the recombination of the phootoinduced e^--h^+. The decrease of emission could be attributed to the electron scavenging effect of Nb which acts as an electron acceptor. This also might be due to transfer of electrons in CB of semiconductor to elecron acceptor in the solution. Figure 4.9(d) illustrtaes the comparison between PL spectra of TiO_2 and Nb-doped TiO_2.

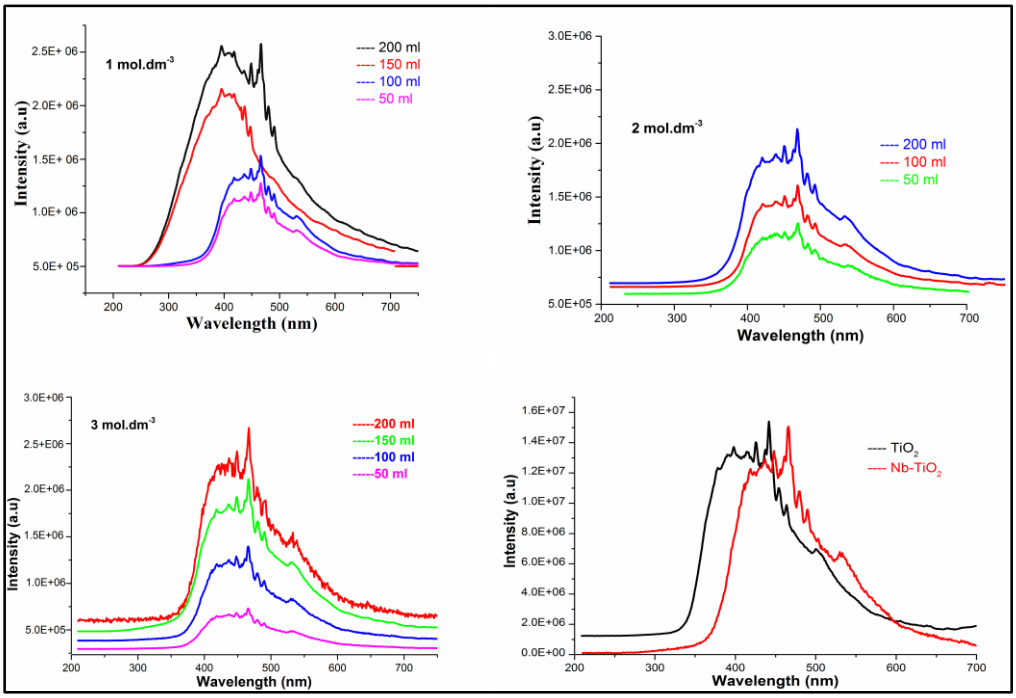

Figure 4.9: PL spectra of a)1 mol.dm^{-3} TiO_2 b) 2 mol.dm^{-3} TiO_2 c) 3 mol.dm^{-3} TiO_2 d) Sol-gel TiO_2 and Nb-doped TiO_2

4.2.6. UV- Visible spectra for absorption and band gap studies

Figure 4.10 illustrates the UV-Visible spectra of the various synthesised nanomaterials. The absorption edges were 410.2 nm, 410.7 nm and 409.05 nm for Nb-doped TiO_2. TiO_2 and P25. For P25, absorption onset was 410.7 nm which reduced to 410.2 nm in Nb-doped TiO_2 composite. This might be due to the crsytallite size and phase of the sample. Thus, there is a blue shift with respect to commercial TiO_2 and a red shift with sol-gel TiO_2 was observed. The red shift attributes to the increase in band gap. Tauc plot was used to calculate the corresponding bandgap energies of the photocatalysts. A plot between (F (R). hν) $^{1/2}$ versus hν. F (R) the Kubelka–Munk function was obtained from reflectance spectra where FR= $(1-R)^2/2R$ equation and hν is the photon energy [58]. After doping, the bandgap decreased and shifted towards the visible area. Tauc's plot for pure TiO_2, Nb-doped TiO_2 (0.04 M, 0.08 M) is plotted in figure 4.2.10. It has been observed that the band gap energy of P25 is 3.23, TiO_2 is 3.21 and 3.1 for doped TiO_2. It was observed that band gap of TiO_2 was greater than commercial TiO_2. With the doping by Nb, band increased and thus, shifted more towards visible region.

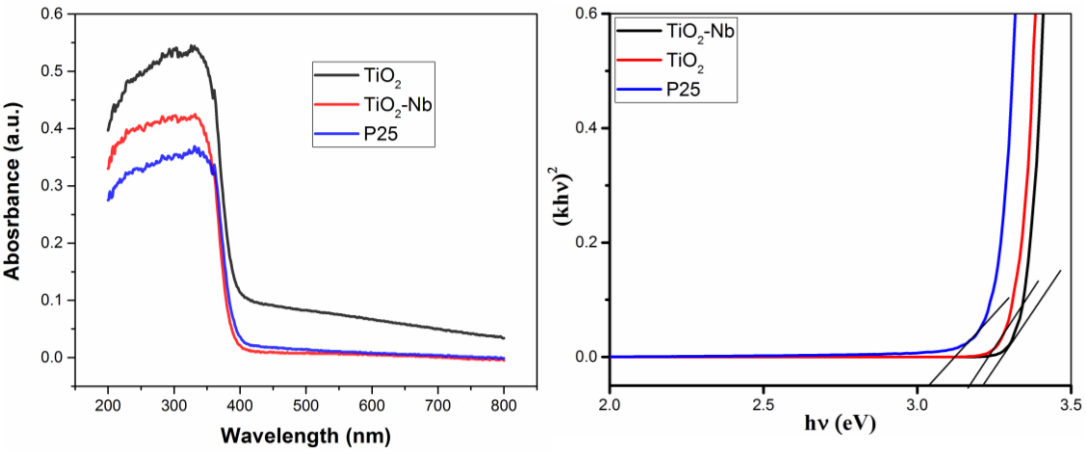

Figure 4.10: UV-Visible spectra and band gap of the various synthesised nanomaterials

4.3. Photocatalytic Reduction of CO2

Photocatalytic reduction of CO_2 has been done on TiO_2 photocatalyst under ambient conditions using 15 W UV lamp as light source. Product formation was analysed by HPLC. The HPLC chromatogram demonstrates the presence of methanol. The compound of interest i.e. methanol must be eluted at 19 min in compliance with the methanol standard. Figure 4.11 shows the standard peak for methanol. Along with methanol, formaldehyde and few other compounds were also eluted. No methanol was produced by TiO_2 (hydrolysis). Figure 4.12 show the HPLC chromatogram to prove the same. This might be due to its small surface area and very high crystallite size. This clearly states that the mode of synthesis of catalyst plays an important role in photocatalytic activity.

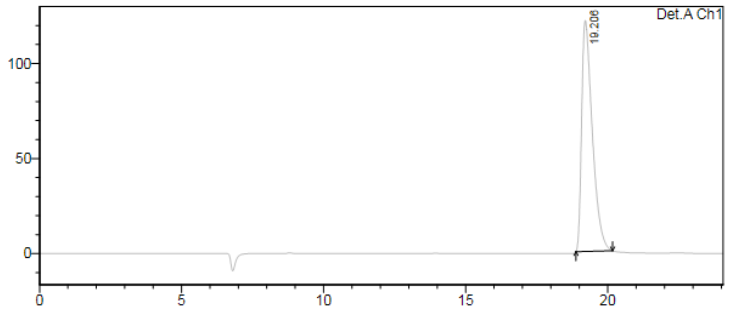

Figure 4.11: Chromatogram for methanol standard eluted at 19 min

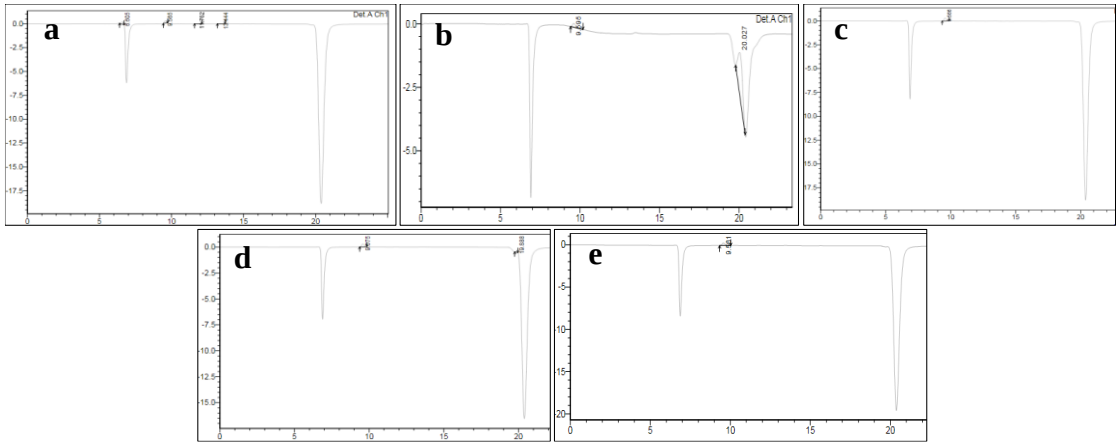

Figure 4.12: HPLC Chromatogram of TiO_2 (Hydrolysis) a) dark b) Without CO_2, CO_2 supplied for c) 1hr d) 2hr e) 3hr

However, with the TiO_2 synthesised by sol-gel method, low yield of methanol was observed. After the calculations done by the quantitation method, 0.15 µg/ ml yield of methanol was observed when CO_2 was supplied continuously for 2 hours. Thus, optimum reaction conditions were CO_2 supplied for 2 hours along with stirring rate at 600 rpm. There should always be a competitive adsorption of CO_2 and H_2O on the active sites of the catalyst [32]. Figure 4.13 shows the HPLC chromatogram for TiO_2 (sol-gel). At first hour, there was no equilibrium attained at the active site for adsorption. After, continuous supply of CO_2, an optimum equilibrium was set at 2 hr that lead to the photoreduction of CO_2. Again, at the third hour, the equilibrium is disturbed and no photoreduction was observed. Though, this was quiet low as compared to the investigations done by Wu et al [32]. They used copper doped TiO_2 to produce methanol from CO_2. Their process gave a yield of 0.45 µgm/ml that was higher than our study. However, in the investigations of Anpo et al and Wu et al, produced a lower yield of 0.08 µg/ ml and 0.06 µg/ ml as compared to our work [59] [60].

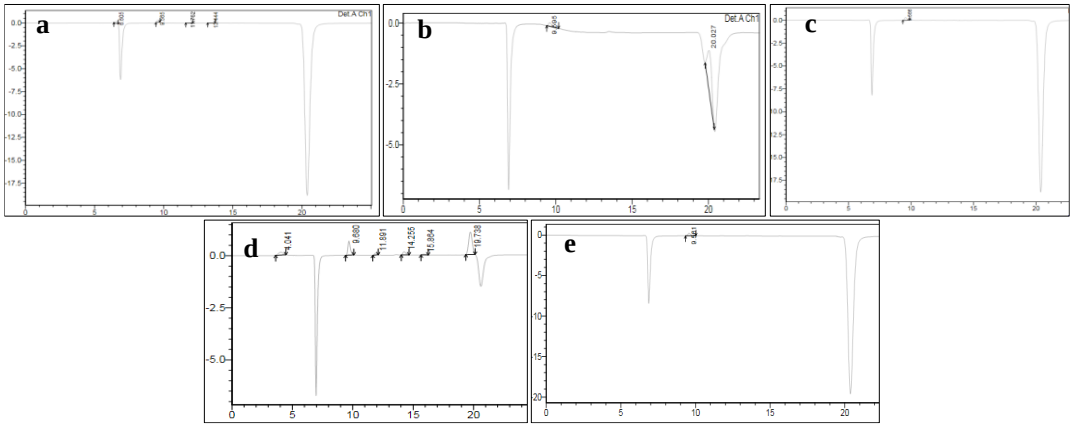

Figure 4.13: HPLC chromatogram of TiO_2 (sol-gel) a) dark b) Without CO_2, CO_2 supplied for c) 1hr d) 2hr e) 3hr

In order to increase the yield we attempted for doping of the material and increase the photocatalytic activity of TiO_2. However, there was no production of methanol when we used the Nb-doped TiO_2 with various concentration. Figures 4.14 and 4.15 illustrate the HPLC chromatogram for TiO_2-Nb (0.04M) and TiO_2-Nb (0.08M) This could be due to saturation of more ions in the solution that would have promoted recombination of electron and hole pair, thus no or very low photocatalytic activity of the material was observed. formation of surface hydroxyls of TiO_2 enhance the adsorption of CO_2 on the surface, thus photoreduction process would enhance [61]. Nb^{4+} ions may prevent the formation of surface hydroxyls of TiO_2 and reduce the photocatalytic efficiency of TiO_2.

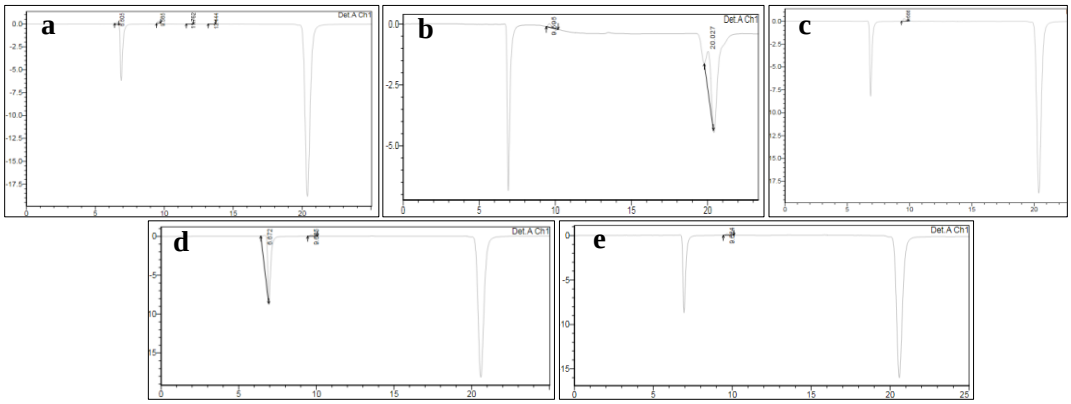

Figure 4.14: HPLC chromatogram of TiO_2- Nb (0.04M) a) dark b) Without CO_2, CO_2 supplied for c) 1hr d) 2hr e) 3hr

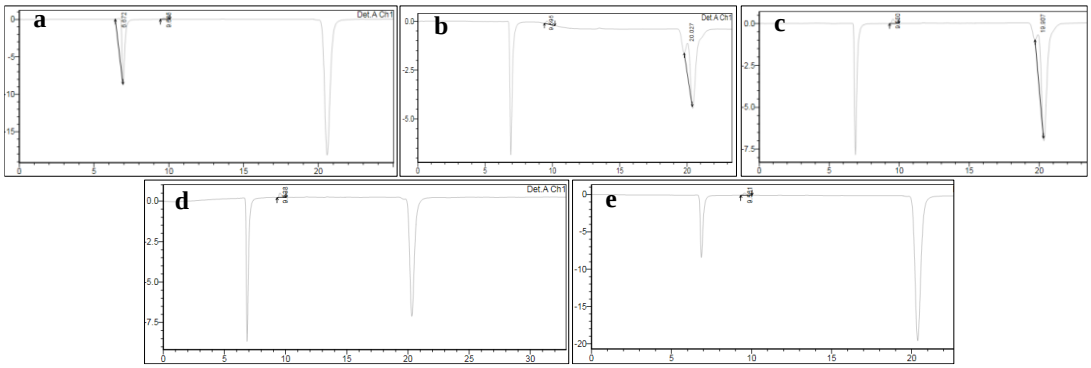

Figure 4.15: HPLC chromatogram of TiO_2- Nb (0.08 M) a) dark b) Without CO_2, CO_2 supplied for c) 1hr d) 2hr e) 3hr

However, there was no methanol production when photocatalytic reduction by TiO_2- Nb (0.04 M) and TiO_2- Nb (0.08 M) but a small peak of formaldehyde was observed at 9.6 minutes. This would explain that Nb-doped TiO_2 exhibited a low photocatalytic activity but was not efficient to carry the reaction upto methanol production level.

Chapter 5

Conclusion

CO_2 is a stable compound and reducing it into valuable products is challenging. There are many hurdles to be crossed like activation of most stable molecule CO_2 and its simultaneous conversion. Photocatlytic conversion takes place under mild pressure and temperature with no specific requirements, thus makes it the most conventional methos to remove CO_2 from environment. Photocatalytic reduction of CO_2 on most commonly used photocatalyst, titanium dioxide, has the great potential to become a promising unconventional source of energy. In this research, an attempt has been made to demonstrate an efficient TiO_2 catalyst along with niobium doping. TiO_2 synthesis was done by two routes, hydrolysis and sol-gel. In hydrolysis method, various concentration from 1 $mol.dm^{-3}$ to 3 $mol.dm^{-3}$ and volume from 50 ml to 200 ml. Anatase phase increased with the increase in volume. The same was the trend in increase of photoluminenscence. Sol-gel proved to be a better photocatalyst with a lower size range of 40-60 nm than hydrolysis method that range from 40-90 nm. The photo reduction of CO_2 with H_2O was efficaciously accomplisedd in a laboratory scale photoreactor with TiO_2 and TiO_2-Nb catalysts. The maximum methanol yield amongst all the catalysts was 0.15 μgm/ml by using TiO_2 (sol-gel) under UV irradiation. Compared with other catalysts proved to be a better photocatalyst. Doping had no positive impact on photoreduction of CO_2 to methanol. All in all, a successful demonstration of material synthesis and its application in photoreduction of CO_2 was achieved.

Bibliography

[1] X. Xiaoding and J. A. Moulijn, "Mitigation of CO_2 by Chemical Conversion: Plausible Chemical Reactions and Promising Products," *Energy & Fuels,* vol. 10, pp. 305-325, 1996.

[2] L. H. Ziska, P. R. Epstein and W. H. Schlesinger, "Rising CO_2, Climate Change, and Public Health: Exploring the Links to Plant Biology," *Environmental Health Perspectives,* vol. 117, no. 2, pp. 155-158, 2009.

[3] Aresta, Michele and E. Giorgio Forti, "Carbon dioxide as a source of carbon," *Reidel,* 1987.

[4] W.-N. Wang, J. Soulis, Y. J. Yang and P. Biswas, "Comparison of CO_2 Photoreduction Systems: A Review," *Aerosol and Air Quality Research,* vol. 14, pp. 533-549, 2014.

[5] M. A. Scibioh and B. Viswanathan, "Electrochemical Reduction of Carbon dioxide: A Status Report," *Proc Indian National Science Academy,* vol. 70, pp. 407-462, 2004.

[6] Z. Jiang, T. Xiao, V. L. Kuznetsov and P. P. Edwards, "Turning carbon dioxide into fuel," *Phil. Trans. R. Soc. A,* vol. 368, pp. 3343-3364, 2010.

[7] C. Song and W. Pan, "Tri-reforming of methane: a novel concept for catalytic production of industrially useful synthesis gas with desired H_2/CO ratios," *Catalysis Today,* vol. 98, pp. 463-484, 2004.

[8] Scibioh, M. Aulice and B. Viswanathan, "Electrochemical reduction of carbon dioxide: a status report," *In Proc Indian Natn Sci Acad,* vol. 70, pp. 1-56, 2004.

[9] J. Tollefson, "How green is my future?," *Nature,* vol. 473, pp. 134-135, 2011.

[10] K. Koci, L. Obalova and Z. Lacny, "Photocatalytic reduction of CO_2 over TiO_2 based catalysts," *Chemical Papers,* vol. 62, no. 1, pp. 1-9, 2008.

[11] V. P. Indrakanti, J. D. Kubicki and H. H. Schobert, "Photoinduced activation of CO_2 on Ti-based heterogeneous catalysts: current state, chemical physics-based insights and outlook," *Energy & Environmental Science,* vol. 2, no. 7, pp. 745-758, 2009.

[12] S. H. Deulkar, H. J. Yo and J. L. Huang, "Tem-Based Investigations on Cvd-Assisted Growth of ZnO Nanowires Inside Nanochannels of Anodized Aluminum Oxide Template," *International Journal of Nanoscience,* vol. 9, no. 3, pp. 225-235, 2010.

[13] T. Inoue, A. Fujishima, S. Konishi and K. Honda, "Photoelectrocatalytic reduction of carbon dioxide in aqueous suspensions of semiconductor powders," *Nature,* vol. 277, pp. 637-638, 1979.

[14] Q. Zhang, W. Han, Y. Hong and J. Yu, "Photocatalytic reduction of CO_2 with H_2O on Pt-loaded TiO_2 catalyst," *Catalysis Today,* vol. 148, p. 335–340, 2009.

[15] P. Li, Ouyang, S.X., G. Xi, T. Kako and J. Ye, "The Effects of Crystal Structure and Electronic Structure on Photocatalytic H2 Evolution and CO_2 Reduction over Two Phases of Perovskite-Structured NaNbO3," *Journal of physical chemistry C,* vol. 116, p. 7621–7628., 2012.

[16] K. Rajalakshmi, V. Jeyalakshmi, K. R. Krishnamurthy and B. Viswanathan, "Photocatalytic reduction of carbon dioxide by water on titania: Role of photophysical and structural properties," *Indian Journal of Chemistry-Part A Inorganic Physical Theoretical and Analytical,* vol. 51, no. 3, p. 411, 2012.

[17] G. Dey, A. Belapurkar and K. Kishore, "Photocatalytic reduction of carbon dioxide to methane using TiO2 as suspension in water," *Journal of Photochemistry and Photobiology A: Chemistry,* vol. 163, p. 503–508, 2004.

[18] S. Krejcikova, L. Matejova, K. Koci, Obalova, L. Matej, L. Capek and O.Solcova, "Preparation and characterization of Ag-doped crystalline titania for photocatalysis applications," *Applied Catalysis B:Environmental,* Vols. 111-112, pp. 119-125, 2012.

[19] T. Nguyen and J. Wu, "Photoreduction of CO2 in an optical fiber photoreactor:effects of metals addition and catalyst carrier," *Applied Catalysis A: General,* vol. 335, p. 112–120, 2008.

[20] Z. Zhao, J. Fan, M. Xie and Z. Wang, "Photocatalytic reduction of carbon dioxide with in-situ synthesized $CoPc/TiO_2$ under visible light irradiation," *Journal of Cleaner Production,* vol. 17, p. 025–1029, 2009.

[21] K. Adachi, K. Ohta and T. Mijuma, "Photocatalytic Reduction of Carbon-Dioxide to Hydrocarbon Using Copper-Loaded Titanium-Dioxide," *Solar Energy,* vol. 53, pp. 187-190, 1994.

[22] W. Wang, W. An, B. Ramalingam, S. Mukherjee, D. Niedzwiedzki, S. Gangopadhyay and P. Biswas, "Size and Structure Matter: Enhanced CO_2 Photoreduction Efficiency by Size-Resolved Ultrafine Pt Nanoparticles on TiO_2 Single Crystals.," *Journal of American Chemical Society,* vol. 134, p. 11276–11281, 2012.

[23] M. Hamadanian, A. Reisi-Vanani and A. Majedi, "Preparation and Characterization of S-doped TiO_2 Nanoparticles, Effect of Calcination Temperature and Evaluation of Photocatalytic Activity," *Materials chemistry physics,* vol. 116, pp. 376-382, 2009.

[24] W. J. Ong, L. L. Tan, S. P. Chai and S. T. Yong, "Graphene oxide as a structure-directing agent for the two-dimensional interface engineering of sandwich-like graphene–gC 3 N 4 hybrid nanostructures with enhanced visible-light photoreduction of CO_2 to methane," *Chemical Communications,* vol. 51, no. 5, pp. 856-861, 2015.

[25] H. Yiming, Y. Wanga, L. Zhang, B. Tenga and F. Maohong, "High-efficiency conversion of CO_2 to fuel over ZnO/g-C3N4 photocatalyst," *Applied Catalysis B: Environmental,* vol. 168, pp. 1-8, 2015.

[26] M. Halmann, "Photoelectrochemical reduction of aqueous carbon dioxide on p-type gallium phosphide in liquid junction solar cells," *Nature,* vol. 275, pp. 115-116, 1978.

[27] Y. P. Xie, G. Liu, L. Yin and H. M. Cheng, "Crystal facet-dependent photocatalytic oxidation and reduction reactivity of monoclinic WO_3 for solar energy conversion," *Journal of Materials Chemistry,* vol. 22, no. 14, pp. 6746-6751, 2012.

[28] Wang, L. G., Pennycook, S. J., & Pantelides, S. T, "The Role of the Nanoscale in Surface Reactions: CO_2 on CdSe," *Physical review letters,* vol. 89, no. 7, p. 075506, 2002.

[29] Q. Liu, Y. Zhou, J. Kou, X. Chen, Z. Tian, J. Gao, S. Yan and Z. Zou, "High-yield synthesis of ultralong and ultrathin Zn_2GeO_4 nanoribbons toward improved photocatalytic reduction of CO_2 into renewable hydrocarbon fuel," *Journal of the American Chemical Society,* vol. 132, no. 41, pp. 14385-14387, 2010.

[30] S. Yan, L. Wan, Z. Li and Z. Zou, "Facile temperature-controlled synthesis of hexagonal Zn_2GeO_4 nanorods with different aspect ratios toward improved photocatalytic activity for overall water splitting and photoreduction of CO2," *Chemical Communications,* vol. 47, no. 19, pp. 5632-5634, 2011.

[31] D. A. H. Hanaor and C. C. Sorrell, "Review of the anatase to rutile phase transformation," *Journal of Materials science,* vol. 46, pp. 857-874, 2011.

[32] J. C. Wu, H. M. Lin and C. L. Lai, "Photo reduction of CO_2 to methanol using optical-fiber photoreactor," *Applied Catalysis A: General,* vol. 296, no. 2, pp. 194-200, 2005.

[33] M. Gratzel, "Photoelectrochemical cells," *Nature,* vol. 414, no. 6861, pp. 338-344, 2001.

[34] C. Burda, X. Chen, R. Narayanan and M. El-Sayed, "Chemistry and properties of nanocrystals of different shapes," *Chemical reviews,* vol. 105, no. 4, pp. 1025-1102, 2005.

[35] L. I. Guohua, C. H. E. N. Dan, Y. A. O. Guoxing, S. H. I. Binbin and M. A. Chunan, "Preparation of WC TiO_2 Core-shell Nanocomposite and Its Electrocatalytic Characteristics," *Chinese Journal of Chemical Engineering,* vol. 19, no. 1, pp. 145-150, 2011.

[36] G. S. Devi, K. S. Kumar and K. S. Reddy, "Effect of pH on Synthesis of Single-Phase Titania (TiO_2) Nanoparticles and its Characterization," *Particulate Science and Technology,* vol. 33, no. 3, pp. 219-333, 2015.

[37] S. A. Ibrahim and S. Sreekantan, "Effect of pH on TiO_2 nanoparticles via sol-gel method," *In Advanced Materials Research,* vol. 173, pp. 184-189, 2011.

[38] H. Y. Zhu, Y. Lan, X. P. Gao, S. P. Ringer, Z. F. Zheng, D. Y. Song and J. C. Zhao, "Phase transition between nanostructures of titanate and titanium dioxides via simple wet-chemical reactions," *Journal of the American Chemical Society,* vol. 127, no. 18, pp. 6730-6736, 2005.

[39] J. H. Lee and Y. S. Yang, "Effect of hydrolysis conditions on morphology and phase content in the crystalline TiO_2 nanoparticles synthesized from aqueous $TiCl_4$ solution by precipitation," *Materials Chemistry and Physics,* vol. 93, no. 1, pp. 237-242, 2005.

[40] M. P. Finnegan, H. Zhang and J. F. Banfield, "Phase stability and transformation in titania nanoparticles in aqueous solutions dominated by surface energy," *The Journal of Physical Chemistry C,* vol. 111, no. 5, pp. 1962-1968, 2007.

[41] D. Zhou, Z. Ji, X. Jiang, D. R. Dunphy, J. Brinker and A. A. Keller, "Influence of material properties on TiO_2 nanoparticle agglomeration," *PloS one,* vol. 8, no. 11, p. e81239, 2013.

[42] M. Wu, J. Long, A. Huang, Y. Luo, S. Feng and R. Xu, "Microemulsion-mediated hydrothermal synthesis and characterization of nanosize rutile and anatase particles," *Langmuir,* vol. 15, no. 26, pp. 8822-8825, 1999.

[43] M. Em, M. Masliana and W. Paulus, "Effect On Used Of Different HCl Molarities to the Characteristic of Nanotitania Powder Produced Via the Hydrothermal Method," *APCBEE Procedia*, vol. 3, pp. 250-254, 2012.

[44] Z. Xu, J. Shang, C. Liu, C. Kang, H. Guo and Y. Du, "The preparation and characterization of TiO_2 ultrafine particles," *Materials Science and Engineering,* vol. 63, no. 3, pp. 211-214, 1999.

[45] W. Zheng, X. Liu, Z. Zhu and Y. L., "Ionic Liquid-Assisted Synthesis of Large-Scale TiO_2 Nanoparticles Controllable Phase by Hydrolysis of $TiCl_4$," *American Chemical Society nano,* vol. 3, no. 1, pp. 115-122, 2009.

[46] S. T. Aruna, S. Tirosh and A. Zaban, "Nanosize rutile titania particle synthesis via a hydrothermal method without mineralizers," *Journal of Materials Chemistry,* vol. 10, pp. 2388-2391, 2000.

[47] G. S. Devi, K. A. S. Kumar and K. S. Reddy, "Effect of pH on Synthesis of Single-Phase Titania (TiO_2) Nanoparticles and its Characterization," *Particulate Science and Technology*, vol. 33, no. 3, pp. 219-223, 2015.

[48] H. Y. Zhu, Y. Lan, X. P. Gao, S. P. Ringer, Z. F. Zheng, D. Y. Song and J. C. Zhao, "Phase Transition between Nanostructures of Titanate and Titanium Dioxides via Simple Wet-Chemical Reactions," *Journal of the American Chemical Society,* vol. 127, no. 18, pp. 6730-6736, 2005.

[49] M. P. Finnegan, H. Zhang and J. F. Banfield, "Phase Stability and Transformation in Titania Nanoparticles in Aqueous Solutions Dominated by Surface Energy," *The Journal of Physical Chemistry C,* vol. 111, no. 5, pp. 1962-1968, 2007.

[50] M. Behnajady and H. Eskandarloo, "Method, Characterization and photocatalytic activity of Ag-Cu/TiO_2 nanoparticles prepared by sol-gel," *Journal of Nanoscience Nanotechnology*, vol. 13, no. 1, pp. 548-53, 2013.

[51] H.-Y. Wang, J. Chen, F.-X. Xiao, J. Zhengb and B. Liu, "Doping-induced structural evolution from rutile to anatase: formation of Nb-doped anatase TiO_2 nanosheets with high photocatalytic activity," *Journal of Materials Chemistry A,* vol. 4, p. 6926, 2016.

[52] A. Teleki, N. Bjelobrk and S. E. Pratsinis, "Flame-made Nb-and Cu-doped TiO_2 sensors for CO and ethanol," *Sensors and Actuators B: Chemical,* vol. 130, no. 1, pp. 449-457, 2008.

[53] S. Phanichphant, C. Liewhiran, K. Wetchakun, A. Wisitsoraat and A. Tuantranont, "Flame-Made Nb-Doped TiO2 Ethanol and Acetone Sensors," *Sensors,* vol. 11, no. 1, pp. 472-48, 2011.

[54] W. Zheng, X. Liu, Z. Yan and L. Zhu, "Ionic Liquid-Assisted Synthesis of Large-Scale TiO_2 Nanoparticles with Controllable Phase by Hydrolysis of TiCl4," *American Chemical Society,* vol. 3, pp. 115-122, 2009.

[55] Hu, W., Li, L., Tong, W., Li, G., & Yan, T, "Tailoring the nanoscale boundary cavities in rutile TiO_2 hierarchical microspheres for giant dielectric performance," *Journal of Materials Chemistry,* vol. 20, no. 39, pp. 8659-8667, 2010.

[56] Z. Teixeira, O. L. Alves and I. O. Mazali, "Structure, thermal behavior, chemical durability, and optical properties of the $Na_2O–Al_2O_3–TiO_2–Nb_2O_5–P_2O_5$ glass system," *Journal of the Ameriycan Ceramic Societ,* vol. 90, no. 1, pp. 256-263, 2007.

[57] A. G. Prado, L. B. Bolzon, C. P. Pedroso, A. O. Moura and L. L. Costa, "Nb_2O_5 as efficient and recyclable photocatalyst for indigo carmine degradation," *Applied Catalysis B: Environmental,* vol. 82, no. 3, pp. 219-22, 2008.

[58] N. Riaz, F. K. Chong, B. K. Dutta, Z. B. Man, M. S. Khan and E. Nurlaela, "Photodegradation of Orange II under visible light using Cu–Ni/TiO_2: Effect of calcination temperature," *Chemical Engineering Journal,* vol. 185, pp. 108-119, 2012.

[59] M. Anpo, H. Yamashita, Y. Ichihashi and S. Ehara, " Photocatalytic reduction of CO_2 with H_2O on various titanium oxide catalysts," *Journal of Electroanalytical Chemistry,* vol. 396, no. 1, pp. 21-26, 1995.

[60] K. Koci, L. Obalova and Z. Lacny, "Photocatalytic reduction of CO_2 over TiO_2 based catalysts," *Chemical Papers,* vol. 62, pp. 1-9, 2008.

[61] Tseng, I. H., Chang, W. C., & Wu, J. C, "Photoreduction of CO_2 using sol–gel derived titania and titania-supported copper catalysts," *Applied Catalysis B: Environmental,* vol. 37, no. 1, pp. 37-48, 2002.

[62] S. G. P. Fageria, "Synthesis of ZnO/Au and ZnO/Ag nanoparticles and their photocatalytic application using UV and visible light," *RSC Advances,* vol. 4, no. 48, pp. 24962-24972, 2014.